DETERMINATION OF STALLING REGION FOR SPECIFIC TURBINE BLADE'S PROFILE

MUHAMMAD SYAHZANI BIN KAMARUDDIN

UNIVERSITI TEKNIKAL MALAYSIA MELAKA

DETERMINATION OF STALLING REGION FOR SPECIFIC TURBINE BLADE'S PROFILE

MUHAMMAD SYAHZANI BIN KAMARUDDIN

This report is submitted
in fulfillment of the requirement for the degree of
Bachelor of Mechanical Engineering (Thermal-Fluids) with Honours.

Faculty of Mechanical Engineering

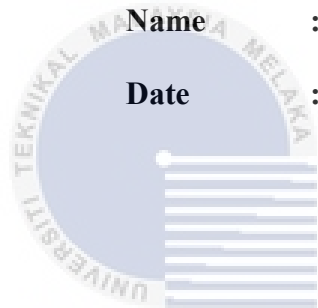**UNIVERSITI TEKNIKAL MALAYSIA MELAKA**

JUNE 2017

DECLARATION

I declare that this project report entitled "Determination Of Stalling Region For Specific Blade Profile" is the result of my own work except as cited in the references

Signature   :   ....

Name   :   Muhammad Syahzani Bin Kamaruddin

Date   :   ....

APPROVAL

I hereby declare that I have read this project report and in my opinion this report is sufficient in terms of scope and quality for the award of the degree of Bachelor of Mechanical Engineering (Thermal-Fluids) with Honours.

Signature   : ....

Name of Supervisor: Dr. Yusmady Bin Mohamed Arifin

Date   : ....

DEDICATION

To my beloved mother and father, supervisor, and friends.

ABSTRACT

Stalling is the phenomena that always happened at the blade profile or airfoil. There is some consideration that need to be taken to curb the stalling phenomena happened to the blade profile such as the blade profile shape, the inlet velocity, and the angle of attack (AOA) for the blade profile. Stalling happened when there is a separation flow at the upper chamber and lower chamber of the blade profile. The separation flow will produce a turbulence flow when it passed the trailing edge of the blade profile. When the region of turbulence flow become larger, the lift coefficient starts to decrease thus, the blade profile had faced the stalling phenomena. The main objective for this study is to find the stalling region for NACA 8415 blade profile at the various angle of attack. This study used computational fluids dynamics (CFD) approach to determine the stalling region. The software that had been used to make the computational fluids dynamics simulation is ANSYS fluent 17.1 version. The analysis for this study only focusing on 2-dimensional analysis geometry only. The fluid is hot air and the inlet velocity is 680m/s at 500°C. The coefficient of lift and drag had been obtained from the CFD simulation and the coefficient of lift and drag vs angle of attack (AOA) had been plotted. From the finding it had been found that the coefficient of lift starts to decrease at the angle of 15°. Thus, the stalling region will be started at angle of 15°.

ABSTRAK

Pegun adalah fenomena yang sentiasa berlaku pada profil bilah. Terdapat beberapa pertimbangan yang perlu diambil untuk membendung fenomena pegun yang berlaku pada profil bilah seperti susuk bentuk bilah, halaju masukan, dan sudut serangan untuk profil bilah. Pegun berlaku apabila terdapat aliran pemisahan di ruang atas dan ruang bawah profil bilah. Aliran akan dipisahkan apabila sudut serang mengalami peningkatan. Aliran pemisahan akan menghasilkan aliran gelora apabila ia melepasi pinggir belakang profil bilah. Apabila kawasan aliran gelora menjadi lebih besar, pekali daya angkat mula berkurangan dengan itu, profil bilah telah mencapai fenomena pegun. Objektif utama kajian ini adalah untuk mencari kawasan pegun untuk profil bilah NACA 8415 pada sudut serangan yang berbeza. Kajian ini telah menggunakan pendekatan perkomputeran dinamik bendalir (CFD) untuk menentukan kawasan pegun. Perisian yang digunakan untuk menjalankan simulasi perkomputeran dinamik bendalir ialah ANSYS fluent versi 17.1. Analisis untuk kajian ini hanya memberi tumpuan kepada geometri analisis 2-dimensi sahaja. Bendalir yang digunakan ialah udara panas dan halaju masukan adalah 680m / s pada 500 ° C. Pekali daya angkat dan seretan telah diperolehi daripada simulasi CFD dan graf pekali daya angkat dan seretan melawan sudut serang telah diplot. Daripada keputusan yang di peroleh, pekali daya angkat mula menurun pada sudut 15 °. Oleh itu, kawasan pegun bermula pada sudut 15 °.

vi

ACKNOWLEDGEMENT

Firstly, the deepest gratitude goes to my parents, Kamaruddin Bin Hashim and Roslinah Binti Yusoh for giving me the advice and motivation during my bachelor studies. The deepest gratitude also goes to my supervisor, Dr. Yusmady Bin Mohamed Arifin for giving me a guidance and advice whenever I faced a problem in this project. Next, I want to thanks to my seminar examiner Dr. Fadhli Bin Syahrial and Mr. Imran Syakir Bin Mohamad for giving a comment and recommendation to finished this project.

I also want to thank to all the lecturer at the faculty of mechanical engineering for giving me their guidance and help during the completion of my final year project report. Last but not least, to all my beloved classmate for providing their knowledge and idea for me to completed my project sarjana muda report and project. Without their help, I will not think that I could doing this alone during my bachelor degree.

TABLE OF CONTENT

LIST OF FIGURES

LIST OF ABBREVIATIONS

Re   Reynold Number

CFD   Computational Fluid Dynamic

2D   two dimensions

3D   three dimensions

RANS   Reynold Average Navier Stoke

BSL   Baseline

TE   Trailing Edge

LE   Leading Edge

SST   Shear Stress Transport

LEV   Leading Edge Vortices

LSB   Laminar Separation Bubble

SB-VAWT   Straight Blade Vertical Axis Wind Turbine

NACA   National Advisory Committee for Aeronautics

C_L	Coefficient of lift
C_D	Coefficient of drag
AOA	Angle of attack
k-ω	k-epsilon
k-ε	k-omega

LIST OF SYMBOLS

p_{gauge}	pressure gauge	pascal
α	angle of attack (AOA)	degree (°)
C_L	coefficient of lift	
K	reduced frequencies	hertz (Hz)
V	velocity of fluid	m/s
l	chord length	m
ρ	density	kg/m^3
μ	dynamic viscosity	kg/m.s
ν	kinematic viscosity	m^2/s

CHAPTER 1

INTRODUCTION

1.0   Background

Stalling is one of the most mutual phenomena that always happened on airfoil profile. Consider the turbine blade is a flat plate, the distinctive average velocity profiles in laminar and turbulent flow are shown in figure 1.1. The velocity profile in turbulent flow is much fuller compared to the laminar flow with a sharp drop near the surface. The turbulent boundary layer can be consisting of four regions that had been characterized by the distance from the wall. The thinnest layer next to the wall where viscous effects are main is viscous sublayer. The velocity profile in this layer is very nearly linear, and the flow is nearly parallel. Next to the viscous sublayer is the buffer layer, in which the turbulent effects are becoming significant, but the flow is still dominated by viscous effects. Above the buffer layer is overlap layer, in which the turbulent effects are much more significant, but still not dominant, (cengel, 2014).
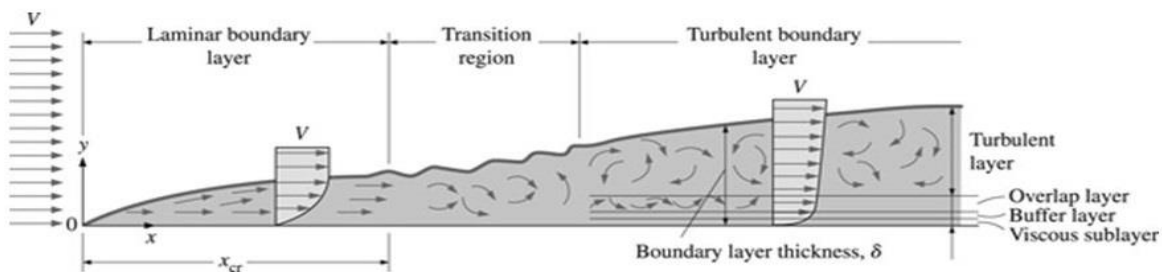
Figure 1.1: development of boundary layer over flat plate, (cengel,2014).

Flow separation occurred at sufficiently high velocities when the fluid stream separates itself from the surface of the body. The location of the separation point is depending on some factors such as the Reynolds number, the surface roughness, and the level of fluctuations in the free stream. It is usually difficult to predict exactly where the separation will occur unless there is a sharp corners or sudden changes in the shape of the solid surface. When the fluid separates from the body, it forms a separated region between the body and the fluid stream. The separated region occurs when the low-pressure region behind the body recirculating on the backflows had occur. The larger the separated region, the larger the pressure drag.

The complete separation over the entire back surface may also occur on the streamlined body at a sufficiently high of angle of attack (AOA) (about $15°$ and above). The flow separation on the top of the surface of airfoil will decreases the lift drastically. This decrease will cause the stalling to happen on the airfoil profile.

An important consequence of flow separation is the formation and shedding of circulating fluid structures. It is known as vortices, and it will fill the empty space that had been produced at the wake region. The periodic generation of these vortices downstream are known as vortex shedding. This phenomenon usually occurs during regular flow over a long cylinders or spheres for Re > 90, (cengel, 2014).

The concept of the stalling for aircraft and steam turbine are not much different. For the aircraft, when the blade suddenly changes its angle, the air flow on the upper surface stops sticking to the surface of the wing. Instead the air turns around and produced a turbulence flow and the irregular vortex will present. The sudden changing f angle will give the effect to the lift of wing from the low pressure to the high pressure on the upper surface of the wing. This phenomenon is known as stall.

2

An aircraft wing will stall, when the shape of the wing tapers off too quickly as the air moves along its general direction of motion. The wing does not change its shape but the angle of the wing will be changed from the general direction of the motion the angle is also known as the angle of attack (AOA). Stall also can be happened if the surface of the airfoil is not completely level and smooth. A dent in the wing or rotor blade, or a piece of self-adhesive tape can will be enough to create the turbulence on the backside of the wing, even the angle of attack (AOA) is small (Krohn, 1998). Figure 2.1 show the turbulence on airfoil at the different angle of attack.
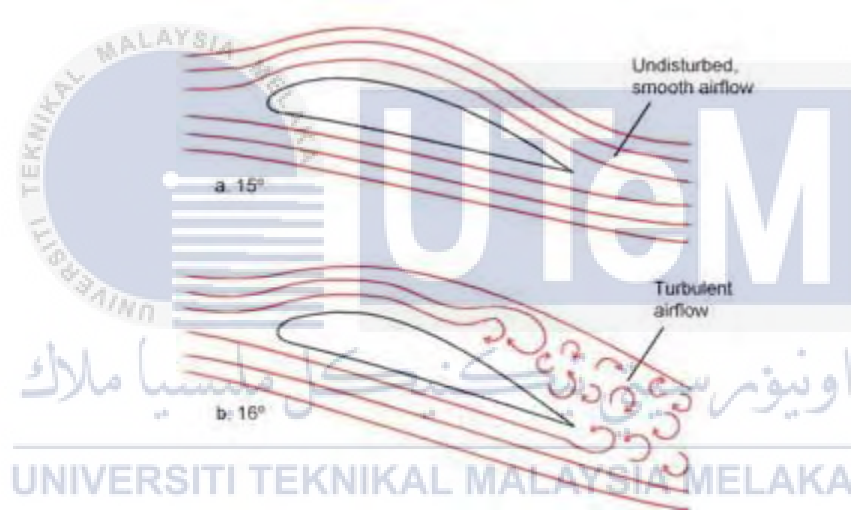
Figure 1.2: the turbulence on airfoil at the different angle of attack (AOA) retrieve fromhttps://www.flitetest.com/articles/how-do-aircraft-fly

1.1 Problem Statement

Steam turbine had been used in steam power plant to generate the electricity. The turbine had been connected to the shaft. The high pressure and velocity of the steam strike the stationary turbine blades and it will cause the turbine to rotate (Gorla & Khan, 2003). Somehow on every airfoil profile, it will produce a turbulence flow at the certain angle (usually above 15º) at the surface of the profile. This problem will cause the stalling happened.

1.2 Objective

The objectives of this project are as follows:

- To obtain stalling point and region for specific blade's profile by adjusting the angle of attack (AOA).

1.3 Scope of Project

The scope of this project is:

1. This project need to use CFD software to simulate the fluid flow through a single blade profile.

2. The investigation involves specific turbine blade profile and various angle of attack (AOA).

3. This project only investigates the behavior of blade profile in 2 dimensional (2-D).

4. The stalling region will be obtained once the graph C_L and C_D against angle of attack (AOA) had been generated.

1.4   General Methodology

The action that need to be carried out to achieve the objectives in this project are listed below:

1. Choosing the profile

    The profile had been chosen based on the literature review reading. Which of profile the most suitable to study.

2. Define the parameter

    The number of angle of attack (AOA), type of airflow, velocity of air flow, and the size of the wind tunnel.

3. Drawing

    The 2-D drawing of the blade profile had been draw by using autocad software.

4. Simulation

    The CFD simulation had been run using ANSYS fluent 17.1 software. The fluid flow through the blade profile had been run from the simulation. From simulation, the coefficient of drag and lift had been found.

5. Result analysis

    From the simulation, the graph of C_L/C_D against AOA had been plotted and the stalling region had been determined. The result consists of the coefficient of lift and drag for a specific angle of attack (AOA).

6. Report writing

    The report of this project had been written at the end of this project.

CHAPTER 2

LITRATURE REVIEW

The literature review showed in this report had been classified into three major domains which is lift coefficient, simulation techniques, and stalling process. The focus is on the formation of the stalling on the steam turbine. The steam turbine consists of bladed components of nozzle, rotating blades and non-bladed component including the inlet and exhaust casing and etc. It is the designer jobs to minimize the energy loss for the component (x.xu et al.,2001). There are many type of turbine one of the example is radial turbine. When talking about designing the radial turbine, the preliminary design work of the radial-inflow turbine is the most important in designing process. The objective of the designing phases is to create an aerodynamic design that will achieve a desired output (Sauret & Gu, 2014). However, sometimes the unsteadiness of the flow on the turbine had been produce by the periodic chopping of the wake region and the formation of the secondary flow vortices (Chaluvadi at al.,2003). There are many applications for the computational fluid dynamics in designing and optimizing turbomachine. It is necessary to obtain accurate prediction of the flow by using the turbulence modelling since the flow of the turbomachine is always turbulent (Lucius & Brenner, 2010).

2.1   Lift Coefficient

Based on the findings from the article (Hoo, et al., 2005), they had produced the plots for the lift coefficient against time. Figure 2.2, had shown that the sinusoidal variation is nearly smooth when the time is reduced. They had expected this since the wing is wavering with the static stall limits, and the flow is therefore predictable to remain attached throughout the pitching cycle. The increasing of K widens the hysteresis loops indicating a larger phase difference with the angle of attack (AOA). The increasing of K will affect the coefficient which is in this case the coefficient of lift will be slightly higher (greater than the steady lift generated at a fix angle of attack). They also had compared the result for theoretical and experimental at different of angle of attack (fig 2.1). It can be see that there is a huge difference between theoretical and experimental result for C_L. The curve shows the wing has stalled beyond the AOA of 10°.
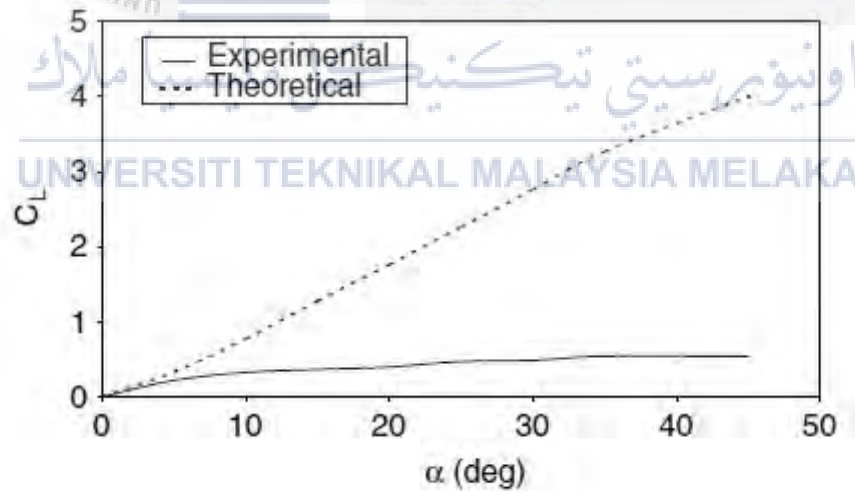
Figure 2.1: Steady state lift coefficient measured at fixed angles of attack compared with theoretical inviscid static lift. Lift recorded when readings attained steady state. Comparison of the curves show the wing has stalled beyond the angle of attack (AOA) of 10° (Hoo, et al., 2005).
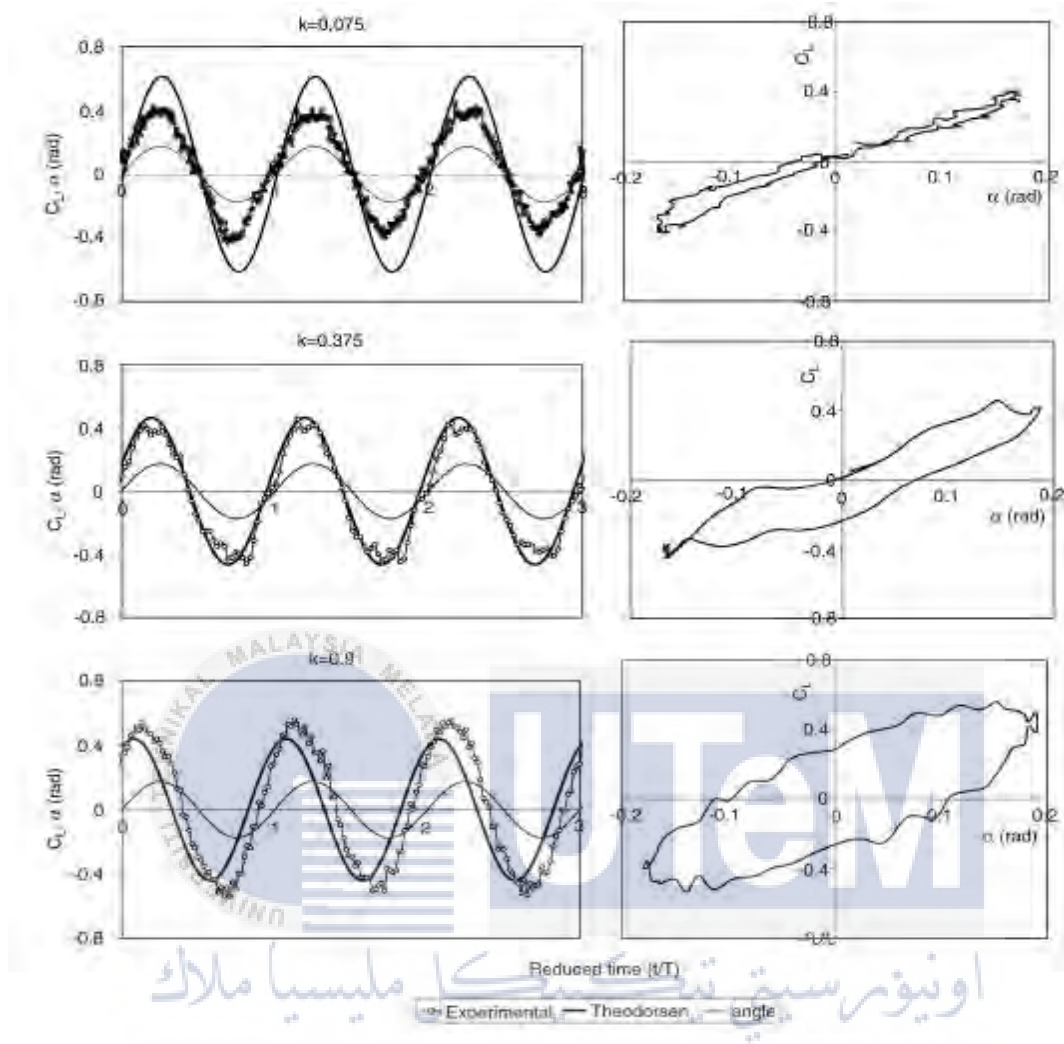
Figure 2.2: Lift force measured for $0 \leq k \leq 0.9$, $-20° \leq \alpha \leq 20°$. Left-hand side—against reduced time, Right-hand side hysteresis plots (clockwise orientation) (Hoo, et al., 2005).

2.2 Simulation Techniques

2.2.1 CFD Comparison

From the investigation of article by Hoo et al., 2005, they had make an improvement on the lift plots that had been simulated by Abkari And Price (2003) by using CFD method. They had been used CFD package (fluent) to perform the numerical simulation on an oscillating wing. Fluent had been used to solve the conservation

8

equation for mass and momentum by using finite volume method to determine the pressure distribution and therefore fluid dynamic forces on the wing as a function of time. The suitable choice of turbulent model is dependent on many factors ranging from flow characteristics to available computing power. They only can apply two model which is k-ε turbulent model and k-ω turbulent model. This is due to the limitations in computing power. Both turbulence model is two equation models in which the solution of two separate transport equations allows the turbulent velocity and length scales to be independently determined. Considering the advantages and disadvantage of each model, the k-ω model was chosen due to its accuracy with the transitional flows.

On the other hands, the article by Costes, et al., 2015 had been make an analysis for unsteady RANS (Reynold average-naiver stoke) for dynamic stall simulation for a 3D finite-span oscillating wing with the ONERA and CFD software. They only considered the fully turbulent computation only. They had compared the result for k-ω model with the experimental data that obtained in the ONERA F2 wind tunnel. Based on this comparison, they had found the important physical features of dynamic stall that had been correctly picked by the numerical model. They also found the differences especially for the stall initiation mechanism. The important weakness that had been found is the computational lies in the small contact between the tip vortex and the flow separation that will cause the leading-edge stall extending close to the wing tip in the simulation. The advantages of the computation are the computation can predict the flow separation closer to the leading edge compared to the observation that had been done in the experiment.

By using CFD method it will provide a shorter time consuming and lower the cost. The unsteady flow field of the aircraft can be predicted by using this method easily. The CFD method is possible to predict the dynamic stall characteristic quickly whether in 2D or 3D condition compared to the experimental method. The CFD method can be used to accomplish the optimization of aerodynamic shape of the rotor air foil if referring to the optimization method (Wang et al., 2015).

Article by Morgado et al., (2016) had comparing the CFD simulation and XFOIL simulation. Both computational fluid dynamics simulations had been performed using steady state solver. The pressure based solver SIMPLE had been used together with a green-gauss cell based discretization. For ANSYS fluent, the second order upwind had been selected as the momentum and turbulence equation of discretization. The Laplacian terms and the pressure equations had been discretized using linear discretization. The convergence monitoring for the relative numerical error of the solution had been set to 1×10^{-8}.

2.2.2 Vortices Method

Article by Akbari & Price, (2003) had investigate on behaviour of the pitching oscillations of NACA 0012 profile. The characteristics of the dynamic stall parameter had been investigated. Comparing to the static stall case, the observation on this research had found that, the pitching oscillation of the air foil had delayed the flow separation to the higher incidences. The separation had been started from the leading-edge and it is follow by the formation and convection of the vortices along the surface of the air foil. They also focus on the trailing-edge behaviour which is common places of vortices will

10

produce. The vortices at the trailing-edge had been shed from the air foil and during the down stroke of the oscillation the secondary vortices had been produced at the upper surface. The flow separation had been delayed due to higher incidences and increasing of the reduced frequency. The normal force coefficient peak had been observed at the higher angle of attack (AOA) with increasing the reduced frequency.

2.2.3 Computational Method

The method that had been used for computational method is boundary condition setup, grid generation, type of viscous model and the simulation setup. For boundary condition setup, the direction of the far-field flow on the stationary air foil had been referred to the sinusoidal equation to get a proper angle of attack (AOA) or wind path for the boundary layer setup. Next, the grid size of the mesh could be variant depend on the location of the air foil. The type of grid that had been used is quadratic mesh for overall of the air foil. On this simulation, the size of the mesh around the leading edge and trailing edge is 60,000 cells and 390 nodes in total. This will give the high-resolution contour on the result later. At the wake region, the size of the mesh had been set to 170 nodes and 80 nodes along the horizontal and vertical lines. At the eroded area, the size of the mesh had been set 10,000 nodes for all simulation.

The viscous model that had been used in this simulation is laminar-turbulent transition. To simulate this model, they had applied a fixed transition point at the lower and upper side of the air foil that will give the effect of transition effects at these two zones. These two zones had been mesh separately with fine and coarse grids. The forward flow zone had been set to laminar and the rest will be a turbulent and will be

11

solved by using turbulent model. All these methods only applied for the static condition.

Since the angle of attack (AOA) of the air foil will be variant, the other approach will be

applied on the air foil later. For the flow condition, the SST k-ω and realizable K-Ɛ model

had been suggested even though, the standard k-Ɛ model have the function for the near-

wall treatment (ANSYS, 2016). On simulation setup, they had chosen the simple

algorithm for coupling the momentum pressure equations. Second-order upwind

differencing scheme had been applied for spatial discretization (Gharali & Johnson,

2012). Figure 2.3 shows the sinusoidal freestream and computational type mesh around

S809 profile.
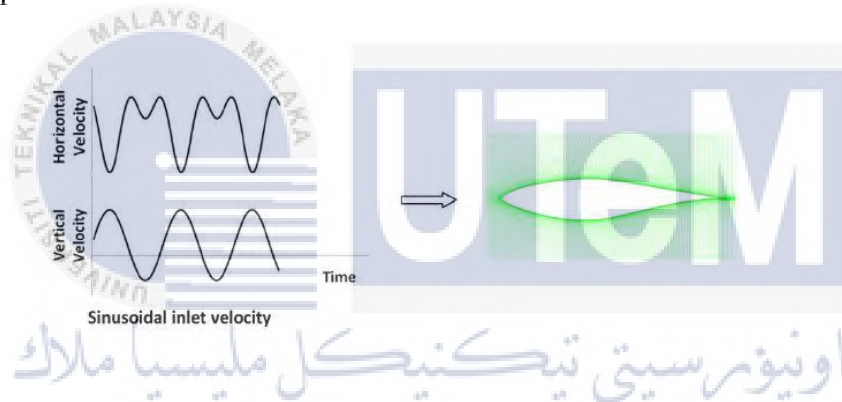
Figure 2.3: Sinusoidal freestream and computational type mesh around S809 airfoil
(Gharali & Johnson, 2012).

Comparing to the dynamic mesh computing, the unstructured grid has a better

geometric in term of flexibility. The dynamic mesh also can be effectively ensuring the

quality of the mesh. Comparing with the structured grid, the structured grid has a better

accuracy thus, to satisfy high quality of mesh, in term of accuracy. The combination of

the structured and unstructured grid had been used on this simulation. Since the blades

operate at a strongly unsteady flow field environment due to the dynamic stall, the k-ω

SST (Shear stress transport) turbulence model had been selected for this simulation. The

k-ω SST turbulence model is a more effective model for the calculation on dynamic stall (Huang, et al., 2015).

In article by Liu, et al., (2014), they had divided the fluid domain into several different zones which is the mesh density for each zone would be different. The mesh had been used is unstructured combining with the triangular element for entire geometry except near-wall region. The size of the mesh near the wall is 512 cells in the chord wise direction. The overall mesh for this study approximately 100,000 nodes. The turbulent model that had been use on this study is SST eddy viscosity model. The transition for the turbulence model need a very fine mesh to get a better result. The condition for the air foil had been set as no-slip condition and the inlet flow had been specified for the upstream boundary domain. The outlet condition reference pressure had been set into $P_{gauge} = 0$ for the downstream boundary of domain.

Menter (1994), had been compared the turbulence model between k-ω SST, k-ω BSL, original k-ω and standard k-Ɛ. The author had been concluded, at the first step a new baseline (BSL) model had been derived and it is utilized the original k-ω model in term of sub- and log-layer. After that, it is gradually switches to the standard k-Ɛ model at the wake region of the boundary layer. On top of that, the k-Ɛ model had also been used for free shear layers' condition. The BSL and original k-ω model are quite identical but, the BSL model had avoids the strong freestream sensitivity of the k-ω model. Both model had been carefully tuned and test in many type of flow to see the difference between each model. Thus, the BSL model had produce a result that is very close to the original k-ω model. The SST model had been suitable used for aerodynamic application due to the significant improvement for all flow that involve adverse pressure gradient.

The new k-ω model had required the high amount of programming effort compared to the original k-ω model.

2.3   Stalling Process

The dynamic stall had been shown to be important in designing the wind turbine. The dynamic stall had produce a large unsteady flow at the wind turbine blade. Wind turbine usually undergoes dynamic stall because of the wind shear, yaw/tilt misalignment, tower passage or atmospheric turbulence. The coefficient of aerodynamic for dynamic stall condition usually are different from the static condition (Pellegrino & Meskell, 2013). The article by Choudhry, et al. (2015) had explained about dynamic stall process in detailed. Based on the article, at the onset rotation, at an angle of attack (AOA) of zero degree (fig. 2.4), the lift formed by the air foil is slightly larger compared to the same air foil at a steady-state conditions. The opening vortex had increase the lift and it induces the additional circulation to the rotating wing. At the onset, the drag formation by the air foil are slightly larger.

Figure 2.4: the air foil at an angle of attack 0° (Choudhry, et al.,2015).

The displaced flow at the trailing edge (TE) interrupts the separated shear layer formation at the trailing edge vortex structure as the air foil pitches. The constant lift had been achieved, this is due to the flow to remain attached during pitch-up even beyond the steady-state

14

stall angle of attack (AOA). Although not at the same rate, the drag of the pitching air foil is constantly increasing. Due to apparent changes in curvature and thickness of the air foil during the pitch-up, non-linear lift curve behaviour had been observed.
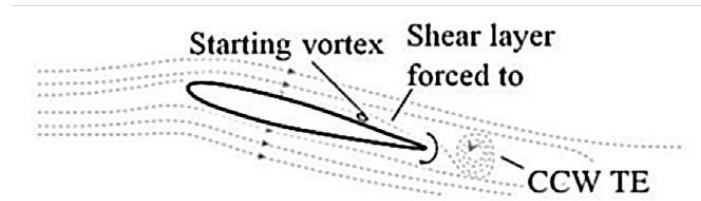
Figure 2.5: the formation of vortex at the trailing edge (Choudhry, et al.,2015)

The shear layer near the trailing edge had been elevated when the trailing edge vortex had leaves the air foil surface. As the angle of attack (AOA) further increases, the reverse-flow regions start to move upstream (fig 2.5). Furthermore, the development of a region of concentrated vorticity that had been bound by a shear layer, had been develops near the leading edge (LE) of the air foil. Due to an apparent flow, a sudden effect of levelling the lift force had been occurs. On the drag flow separation and drag force, there is no effects had been observed.
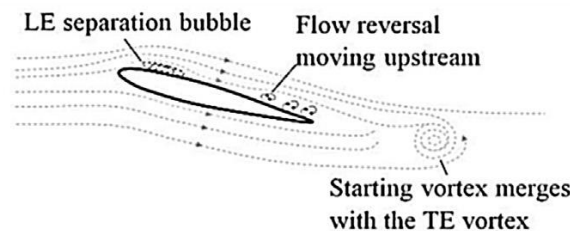
Figure 2.6: the formation of leading edge separation bubble (Choudhry, et al.,2015).

15

Figure 2.6 shows the reverse flow from the trailing edge starts to move towards the leading edge of the air foil when the air foil continues to pitch and the shear layer lift-up at the leading edge had been increasing gradually. Finally, the dynamic stall vortex had been produced, due to the large adverse gradients when the shear layer rolls up. A rapid increase in both lift and drag forces is observed, as the vortex grows in strength due to accumulation of vorticity from the shear layer.
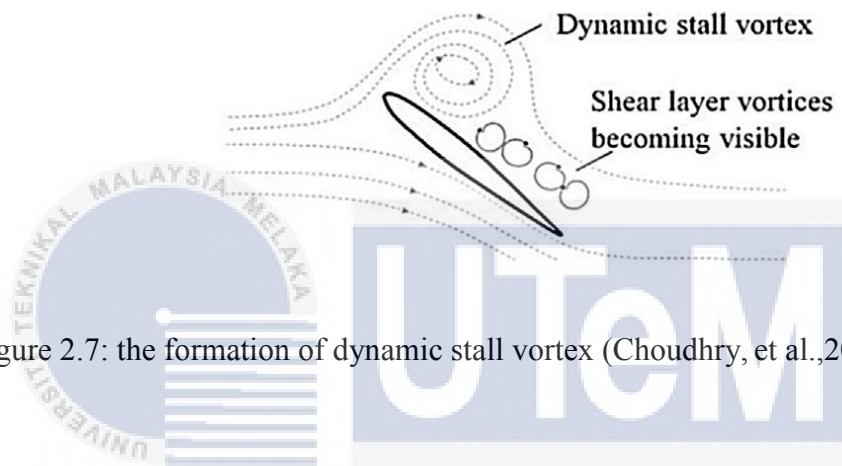
Figure 2.7: the formation of dynamic stall vortex (Choudhry, et al.,2015).

Figure 2.7 shows the formation of dynamic stall vortex as the dynamics stall vortex convicts to approximately at the mid-chord of the air foil, the peaks for the lift and drag forces had been observed. The large-scale flow separation occurs on the air foil and resulting a sudden loss of lift when the dynamic stall vortex leaving the air foil. Due to the leaving of the dynamic stall vortex, the drag at this point had been decreases slightly. Post stall fluctuations in the forces had been observed, due to the secondary and tertiary vortices that are produced after the convection of the primary dynamic stall vortex.

Dynamic stall vortex
convects to mid-chord

Note that the effect of the vortex is not local
and extends to the entire upper surface
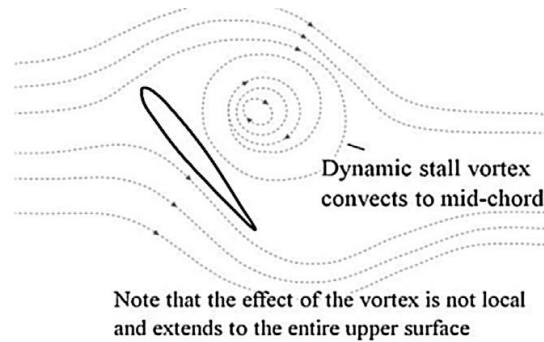
Figure 2.8: the movement of the dynamic stall vortex to the mid-chord
(Choudhry, et al.,2015).

Complete flow separation

Separated DSV

Formation of a TEV
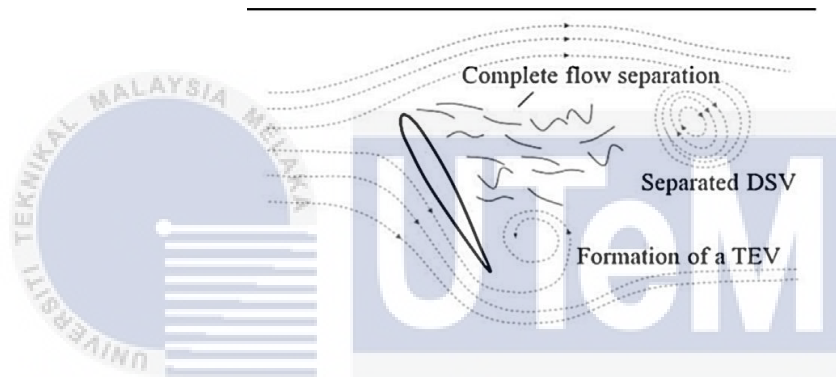
Figure 2.9: the separation of dynamic stall vortex that produced complete flow separation
(Choudhry, et al.,2015).

From the figure 2.8, the dynamics stall vortex had started to leave the mid-chord of the

air foil. The dynamic stall vortex moves towards the trailing edge. When the separated dynamic

stall vortex had leave the trailing edge. The complete flow separation had been produced (fig

2.9). At this stage, the air foil had lost its lift coefficient and the drag coefficient started to

increase. The drag coefficient increases due to the formation of the vorticity at the upper

chamber. The vorticity at the upper chamber had produce a high pressure at the upper chamber

of the air foil thus, the air foil loses its lift. Figure 2.10 had shown the curve for coefficient lift

and drag against the angle of attack.

17
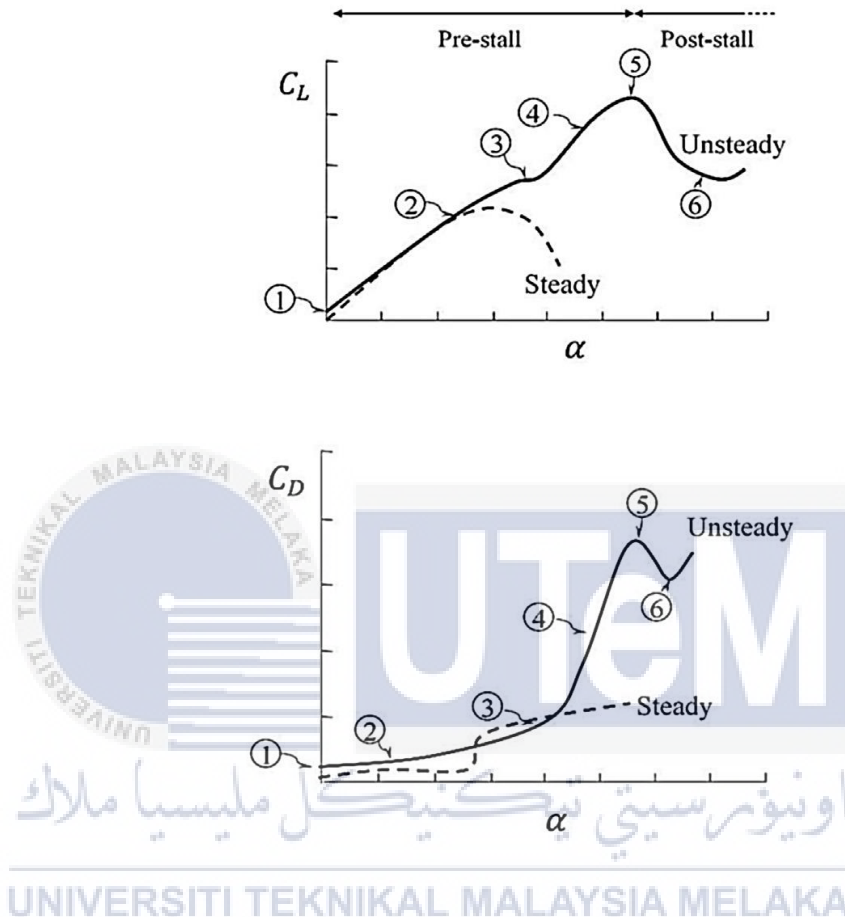
Figure 2.10: the coefficient of drag and lift against the angle of attack (AOA) curve (Choudhry, et al.,2015).

For article by Wang et al., (2012), they had discussed about dynamic stall process for NACA 0012 air foil. Based on the transition SST (shear stress transport) model, the process of the formation and shedding of the LEV (leading edge vortices) that transmits a low-pressure wave sweeping over the aerofoil along the suction surface of the air foil had been known as the deep dynamic stall. At the beginning of the up-stroke phase, the flow is fully attached to the air

foil (see fig. 2.6). On the air foil, there will always be instantaneous streamlines on the air foil surface. At the upper surface of the blade, there is a formation of a very thin flow of reversal layer. The opening of laminar separation bubble cause by the separated shear layer had been produced.

The tiny separation bubble had been detected nearer to the leading edge of the air foil at $\alpha = 15.7^\circ$. At $\alpha = 18.3^\circ$, they had found that the LSB (laminar separation bubble) are close to the turbulence kinetic energy field. At this stage, the leading edge that had been nearer to the boundary layer are still laminar. Based on their findings, the laminar-to-turbulent transition had been produced because the separated still laminar flow is very sensitive to the disturbance. The flow can reattach after the initial transition, because of the capability of the turbulent boundary layer to convey the pressure gradient.

The LSB (laminar partition bubble) develop and travels towards the trailing edge of the air foil as α increase and at $\alpha = 20.6^\circ$ the LSB has crossed over roughly 33% of the suction surface with a low-pressure region inside it. At this occurrence, the LSB has totally transformed into the LEV (leading edge vortices). At this stage. There is a thick turnaround of flow separation layer behind the LEV on the upper surface of the air foil. The slope of the computed C_L curve shows a sudden increase at $\alpha = 22.5^\circ$.

At $\alpha = 23.86^\circ$, the C_L is approaching its maximum value and the LEV has enclosed the whole suction surface (see fig. 2.7). When the LEV spans completely over the air foil, the C_L reaches its highest value but it is still attached to the suction surface and the front part of the LEV has break into two small vortices. The LEV begins to separate from the air foil surface and induces a vortex at the trailing edge, from the low-pressure wave during the further convection of the LEV downstream. The detachment of the LEV, cause an increment in the pressure on the

19

upper surface leading to a significant decrease in the value of C_L. At the maximum angle of attack $\alpha = 25^o$, the LEV becomes unclear and the trailing edge vortex has grown to be very large and it rolled up to the upper surface of the air foil.
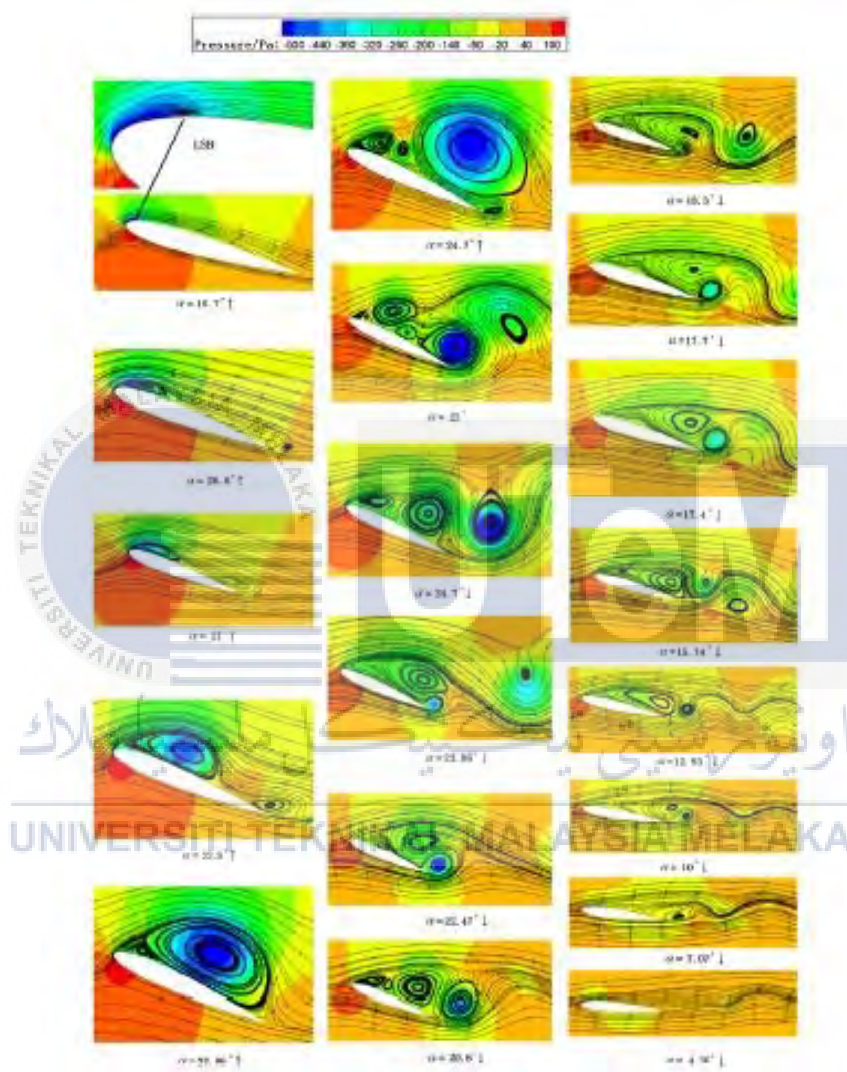
Figure 2.11: pressure field superimposed on the instantaneous streamlines computed using the transition in SST model (Almohammadi, et al., 2015).
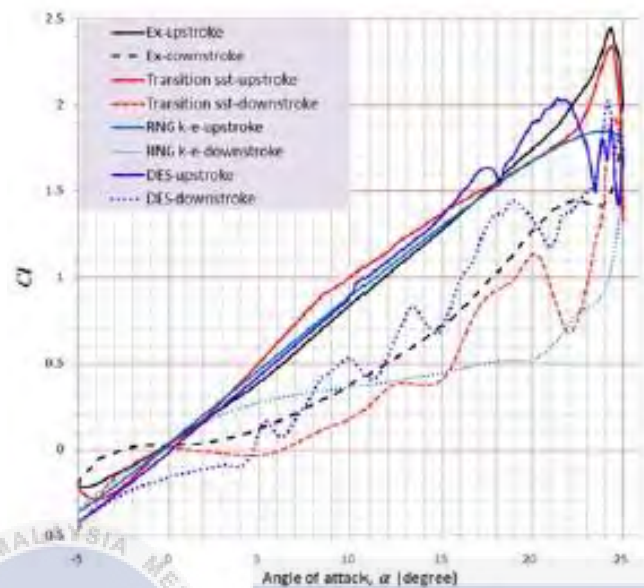
Figure 2.12: the lift coefficient using various model (Almohammadi, et al., 2015).

The article by Almohammadi, et al., (2015), had discussed about the dynamic stall process. On this paper, they had used two turbulence model that is SST K-ω and the transition SST model (see fig 2.12). Based on this paper they had found that there is a two process of combination in dynamic stall in SB-vawts (straight blade vertical axis wind turbine). Based on their finding (see fig. 2.11) they had found that, the first formation of the vortex had been found near the trailing edge of the air foil that had circulates towards the leading edge. The second creation of the leading-edge vortex had moves towards the trailing edge. The combination of the two vortices will produce a large vortex that sheds into wake. On this article, they had also found that the transitional effect that had been vital on predicting the dynamics stall. By using the transitional model for the SST K-ω model, the prediction of the stall is earlier than the expected.

21

Where article by Geissler & Haselmeyer, (2006), had studied about the dynamic stall on the OA312 air foil. This study had been run by using experimental method. They had separated the cases into 3 cases which is free transition and fully turbulent at smaller Mach number (M=0.2) and free transition at higher Mach number (M=0.4). The experiment had been carried out using VAG test stand. The cycle of hysteresis at the different pressure had been compared with the numerical solution that had been made. The calculation had been done in turbulent or transitional mode by applying the transition model. Based on their finding, they had found that the development and the extension from rear to front turbulent separation area had plays a huge impact for dynamic stall onset process. The separation area that had reach the leading edge had produced the displacement effect on the air foil. This effect will shift the vorticity to the outer of the flow.

2.3.1 Laminar Separation Bubble (LSB)

Article by kel & Genc, (2016) had been studied about the effect of the perpendicular acoustic excitation on laminar separation bubble, aerodynamic and stall characteristics over NACA 2415. These studied had been investigated at low Reynolds number with various angle of attack (AOA). Based on their findings, they had found that the LSB had been formed at a lower angle of attack (AOA). The LSB had been shorten due to the perpendicular acoustic excitation forced. They had been observed that, the separated flow had been reattached due to the force from the perpendicular acoustic excitation. This had been caused LSB occur and the stall angle had been increased 5° and 4° that had been lead to the increment of the maximum coefficient of lift to 10% and 14%. At Re = 5 x 10^4 and Re = 7.5 x 10^4, the coefficient of drag had been decreased at 25% and 26%. The perpendicular effect of acoustic excitation on the flow

had been reduced at higher Reynolds number. They had found, the maximum and minimum frequency for acoustic excitation. They also had figured out the effective frequencies that had been resonate with the stream wise fluctuations. The flow of the energy provides the separated flow to reattach back and cause large changes in pressure distribution or the reattachment point of the separation bubble that had been occur at lower angle of attack (AOA).

Comparing to the article by Anand & Sarkar, (2016), they had studied about laminar separated flow at the leading edge for -3º to 10º. The chord length for the air foil had been fixed to 1.6×10^5 and the freestream turbulence had been set to 1.2%. The reattachment of the separation bubble had been shift from 18.8% to 47.7% of the chord and producing an enlargement of the length of the bubble from 11.1% to 42.2% with the increasing the angle of attack (AOA) of the air foil. It been found that at angle of 0 deg. The large eddies scale had been appeared in the second-half of the bubble and it shed sometimes to reveals the normal vortex shedding.

CHAPTER 3

METHODOLOGY

3.1 Introduction

This chapter describes the methodology used in this project to obtain data for drag and lift coefficient and the angle of attack (AOA) that will produce turbulence flow that lead to the stalling. Every blade profile has their own capabilities and it is being choose and been used based on the condition. It is important to choose a suitable blade profile in designing the steam turbine, this is because the suitable blade profile will produce less drag, thus increase the efficiency of the steam turbine to produce more energy. The suitable angle of attack (AOA) for the simulation will be referred on the journal reading.

3.2 Research Method

The information on the stalling had been gathered and referred based on the journal, text book, lecture notes, internet sources and lecturer to get the general idea and planning for the project. At the preliminary stages, the rough flow chart had been produced and had been purposed to the supervisor to get the overall flow of the project. All information had been gathered based on the title of the project and the literature review had been made based on the journal reading to get better understanding for the topics. The apparatus that had been used for this project is computer/ laptop that had been completely installed ANSYS for simulation and

autocad software for drawing the geometry of NACA 8415. The NACA 8415 had been generated from the airfoiltools.com to ensure the shape that had been obtain as desired.

Based on the flow chart in figure 3.1 below, the project had been started by gathering the information and produce a literature review from the reading. After make, a review from the reading, the suitable of blade profile had been selected based on the reading. The NACA 8415 had been choose as the profile for this project to study the stalling behaviour on this profile. The profile had been generated from the airfoiltools website and the website had generated the coordinates for the blade profile. The coordinates had been inserted into the autocad by using spline coordinates. The CAD drawing had been save in. IGES format to make sure it can be run on ANSYS fluent for CFD simulation. After obtaining the result from the simulation, the result had been analyst based on knowledge from the reading, whether the result is significant or not. If the result is not significant, the simulation had been run once again. If the result is significant, the conclusion and the limitation of the profile had been stated.
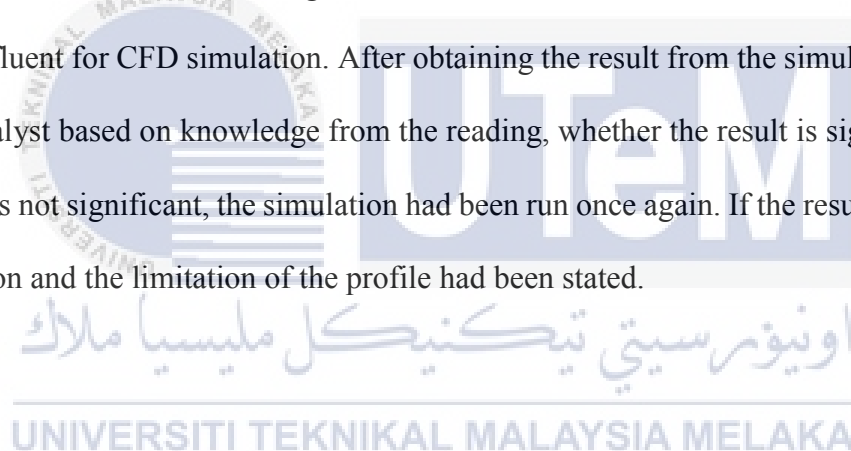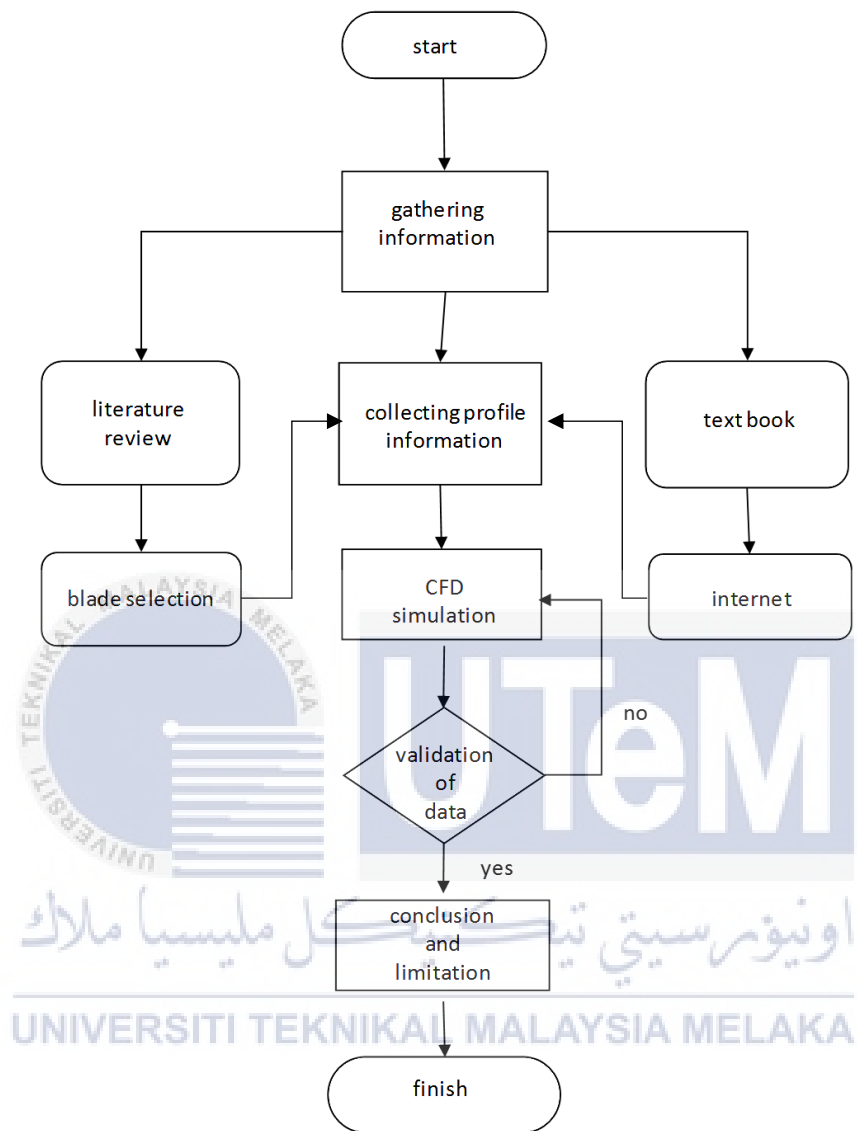
Figure 3.1: flowchart

3.3   Determining the Suitable Blade Profile and Parameter

Figure 3.2 had been shown the Nomenclature of blade profile. The blade profile is chosen based on the internet review, literature review and turbomachinery books reading. As had been mention earlier, the blade profile that is chosen for this project is NACA 8415. Most of the literature study on stalling only focusing on wind turbine blade which is NACA 0012, this blade profile has a symmetry and a flat surface at the lower chamber. NACA 8415 is chosen because the profile had been widely used in steam turbine application thus, it is suitable to be used on this project. For steam turbine application, the profile should have a curve at the lower chamber to produce a force to rotate the turbine. Some of the parameter of the profile had been fixed earlier. The parameter that had been fixed is the size of test section, chord length for the profile and working fluid. Nevertheless, all these parameters should have the validation first before it been used on this project. The size for a test section is 100cm x 50cm, where the chord length for the blade profile is 10cm. The position of the blade profile should be exactly at the middle of the test section. For the first simulation, the profile had been set at angle of -10º. After that, the angle had been increased 10º for each simulation. On this project, the variation of the angle of attack (AOA) had been taken to get more accuracy in determining the stalling region later. The working fluid that had be used in this project is hot air at 500ºc (773K) and the velocity for the fluid will be 6500 RPM (680.68 m/s).
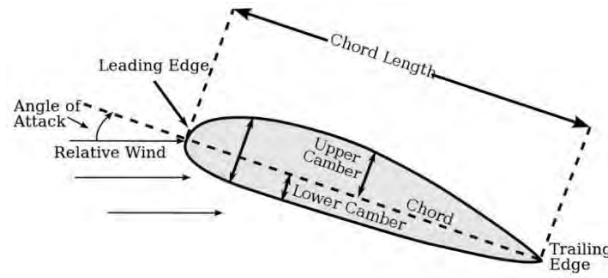
27

Figure 3.2: blade profile nomenclature

3.4   Simulation

3.3.1   Importing Drawing into Workbench

The airfoil profile that had been drawn by using Auto CAD software had been imported to the ANSYS workbench. On the ANSYS software, at the tools box, click on the fluid flow (fluent) and drag it to the project schematic area. The box had been appeared and show the analysis system. The analysis type for this simulation had been set in 2D. After that, the CAD drawing had been import on design modular. The drawing need to be generated first, to ensure there is no problem on the drawing the line body setup (fig. 3.4) need to turn on first and after that generated the drawing. Design modular had shown the line body of the air foil (fig. 3.5). The drawing need to be checked first if there is any missing or unconnected line. The imported drawing need to be place at the middle of the axis in order to make it easier to adjust the angle of attack (AOA) for the next simulation.
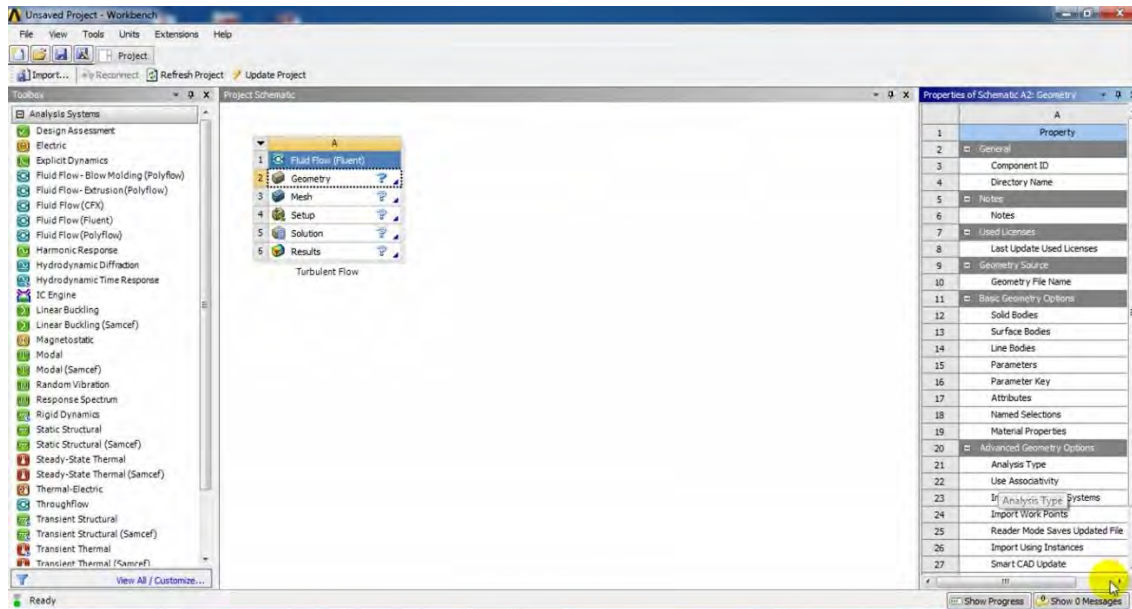
Figure 3.3: ANSYS workbench
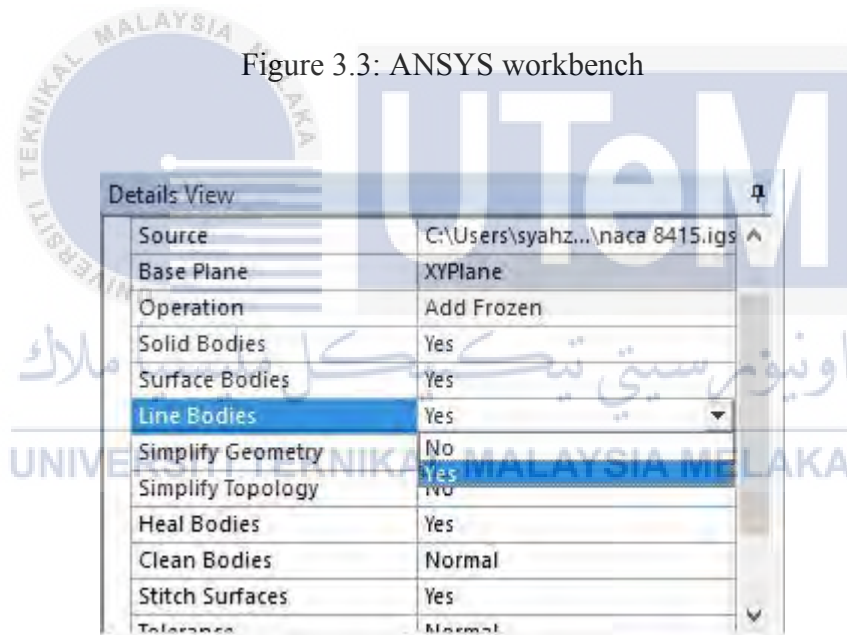
Figure 3.4: line body setting
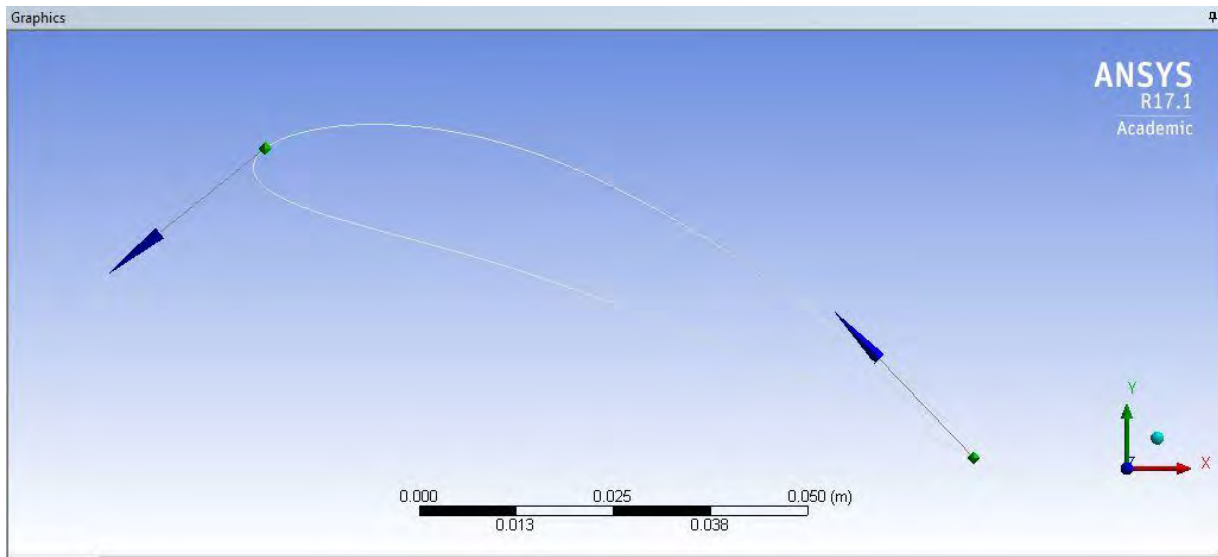
Figure 3.5: the air foil line body

Next, the airfoil need to be placed in the test section by choosing the sketching tab, the drawing can be edited. The size of the test section is 50cm x 100cm as had been mention earlier. After built a test section the line need to be transform into a surface in order to make a mesh later. For the airfoil part, click at the top left corner on the interface and select concept. The display had been shown in figure 19. After that, the surface forms the edges had been selected and at the detailed view section, it will ask to define the geometry. The 2 edges of airfoil part had been selected and the thickness of the surface is 0 meter. After that, click at the generate button to generate the surface, the surface that had been produced had been shown in figure 3.6.
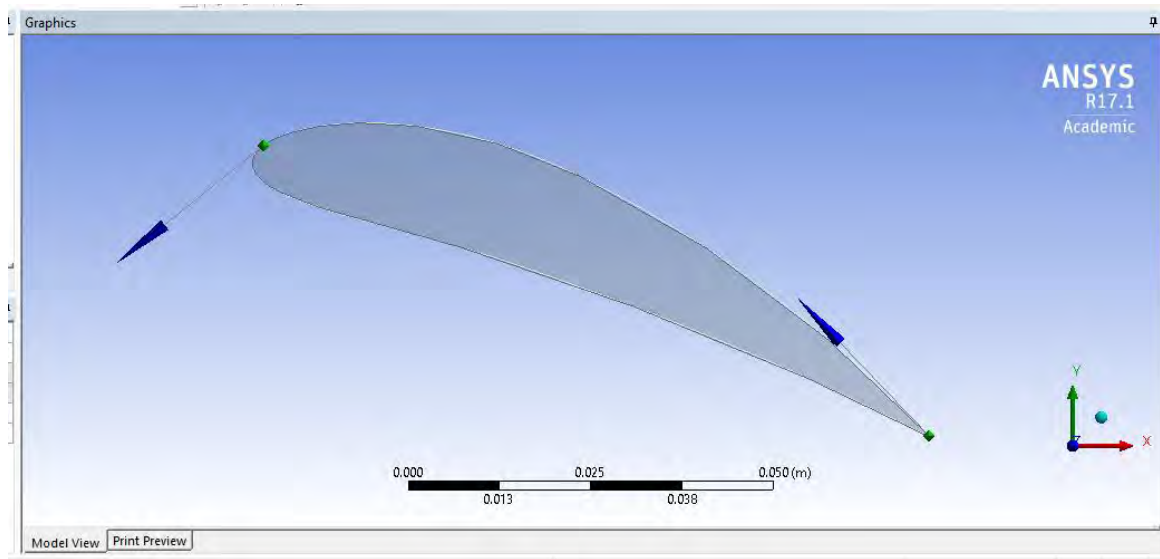
Figure 3.6: surface edges

The test section also need to be set as a surface, by choosing the concept menu at the top left of the interface, the surface forms the sketches features had been selected. On X-Y plane, the test section sketch line had been highlighted. Select apply on the geometry box and set the test section material as add frozen. After that, select generate and it will produce an overlapping surface between the test section and the airfoil. Next, select create at the top left of the interface and choose Boolean. The detailed view menu will display the operation as figure 3.7.
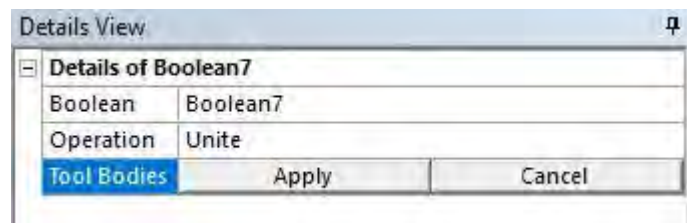
Figure 3.7: Boolean detailed view

3.3.2 Meshing

Meshing is very important in the CFD simulation. To run the simulation, the meshing need to be done first. First, open the mesh modular and the geometry had been imported to the mesh modular. The default mesh had been generated at the surface of the geometry. The sizing for the default mesh is course. The detailed of the mesh had been shown as the figure below.
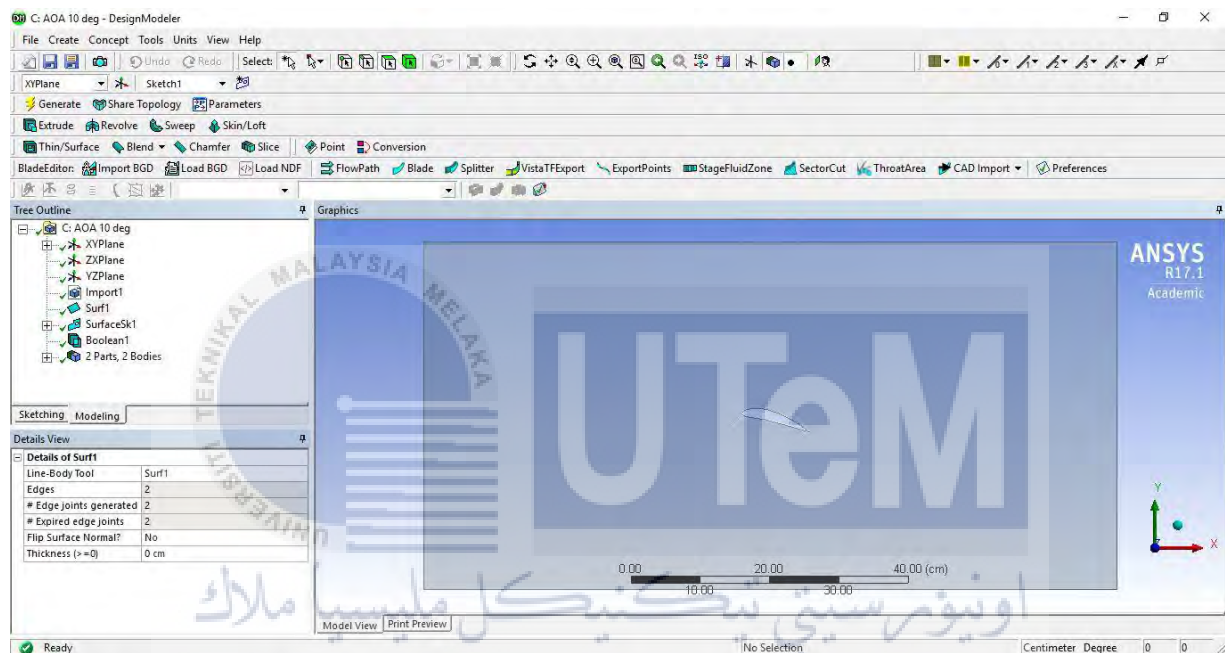
Figure 3.8: result for Boolean operation
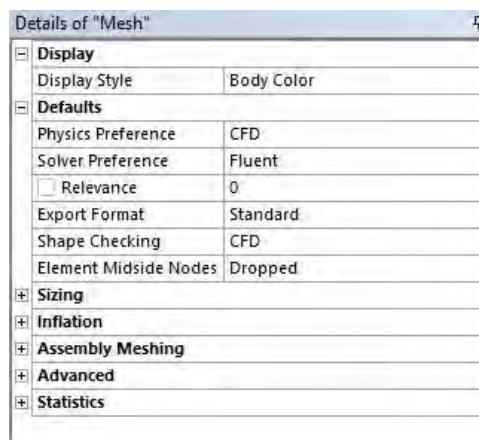
Figure 3.9: example details of mesh

Statistics	
Nodes	1377
Elements	1056
Mesh Metric	None

Figure 3.10: example of node and element

The mesh size need to be set for mesh to cover all the surface of the geometry. The size of meshing had been depended on the region, usually at the edges of the geometry the meshing size usually smaller because it is considered as a critical part for the geometry and need to be focusing. For this project, the fine meshing had been used at the edge of the air foil. At the inlet and outlet of the test section, the course mesh had been used. This is because it is not the important region that need to be focused. The focus of this project is at the airfoil region that had been offset at the middle of these test section. The nodes and element for this geometry is 144739 and 284565 respectively.

3.3.2.1   All Triangles Method

The shape of the default mesh that had been generated was quadrilateral. The quadrilateral shape did not fully cover the air foil shape; thus, it had produce inaccurate result when do the simulation later. Thus, the triangles method had been selected to change the shape of the mesh. The geometry that had been selected is the whole body of the test section geometry and the definition method had been changed from quadrilateral to triangles.

33

Figure 3.11: detail for all triangle method

3.3.2.2 Body Sizing

The body sizing had been selected to standardize all the mesh size. The geometry that had been selected is the whole body of the geometry. On the type section the sphere of influence had been selected and the global coordinate system had been selected as the sphere centre. The size of the radius is 20cm since the height of the test section is 25cm from the airfoil. The element size inside the sphere had been set to 0.5 cm which is smaller than the body sizing element size.

Figure 3.12: detail of body sizing

3.3.2.3   Edge Sizing

The edge sizing had been selected is to size the shape of mesh at the edge nearer to the airfoil. The size for this sizing need to be smaller than the body sizing because this region is considered as the critical region for this geometry. This region is the region that need to be studied in this project. Only one edge had been selected in this mesh, for the first edge sizing the upper chamber had been selected first. The edge sizing had been separated into to part because it easier to differentiate the upper and lower chamber region of the air foil. After set, the setting for the edge the edge sizing, the edge sizing had been duplicated and the lower chamber region had been selected.
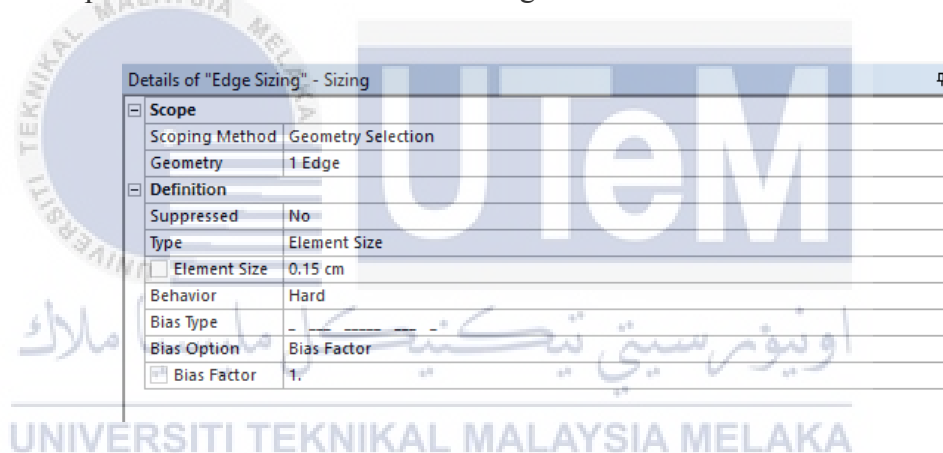
Figure 3.13: detail for edge sizing

3.3.2.4   Inflation

The inflation need to be put on this mesh control because the inflation had produce a boundary layer at the lower and upper edger of the airfoil. The boundary layer is needed in order to see the friction that had been produce at the stationary wall (airfoil wall). The total thickness had been selected as the inflation option and the number of inflation is set to 10 and the maximum thickness of inflation is 0.25 from the airfoil surface.
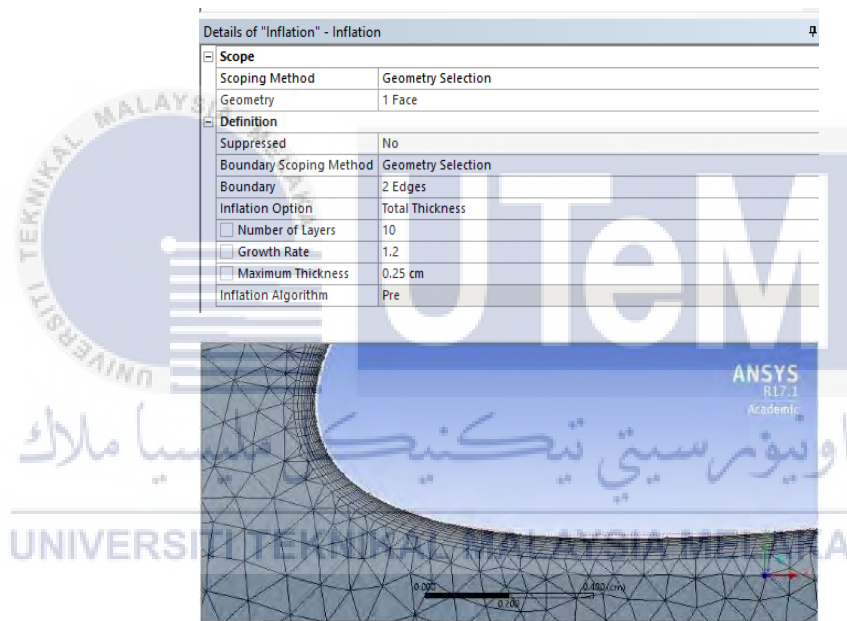
Figure 3.14: detail for inflation

The last step that had been done in meshing is naming the boundary of the geometry. It is important to name the boundary correctly to make sure the programme can understand the name. For example, for upper wall of the test section, the naming should be: upper_wall so that, the programme can read the name correctly. It is the must to naming all the boundary that have in the geometry to avoid error.

36

3.3.3 Solution and Setup

Solution and setup only can be done once the meshing had been finished. Once the fluent had been started it had shown a pop up for the preliminary setting for simulation. The type of the simulation need to set whether in 2D or 3D. For this case, the type of simulation already defined at the geometry which is 2D. At the option check box, the double precision need to be checked and serial option had been selected as an operation selection. Once the preliminary setup had been done the fluent will be start up and the mesh had been load. Click on the info to check the size of the latest mesh. The type of the solver that had been used is density based and the time is steady because the flow did not change with the time. At the model menu, it had shown the model that have in ANSYS fluent. The project is covered only for viscous and energy model. The energy model had been turned on because the simulation is dealing with the temperature. There are many viscous models in ANSYS fluent. The project only focusing on the turbulence model. There are 4 turbulence models in ANSYS fluent which is k-epsilon, k-omega, spalart-almaras and transition SST. To define the flow as a turbulence model, the Reynolds number should be greater than 4000. The calculation Reynold number for this simulation can be calculated as below:

$$\text{Re} = \frac{\rho v l}{\mu} = \frac{v l}{\nu}$$

Where:

v = Velocity of the fluid
l = The characteritics length, the chord width of an airfoil
ρ = The density of the fluid
μ = The dynamic viscosity of the fluid
ν = The kinematic viscosity of the fluid

Figure 3.15: Reynold number formula (courtesy of tutorvista.com)

The Reynold number for this study is exceeding the 4000. So, the flow for the simulation is turbulence. Thus, the turbulence model need to be selected for the simulation. The viscous model that will be used on this project is standard k-epsilon model. The k-epsilon model had been chosen in this project because the k-epsilon model only used small processing capacity compared to the other turbulence model. For the fluid, the hot gas at 500°C temperature had been used as a fluid for inlet of the test section and the boundary condition for upper and lower wall had been set as no slip wall. The inlet velocity had been set as 680m/s. After finish setup, all the boundary condition, the project need to be save first to proceed with the solution.
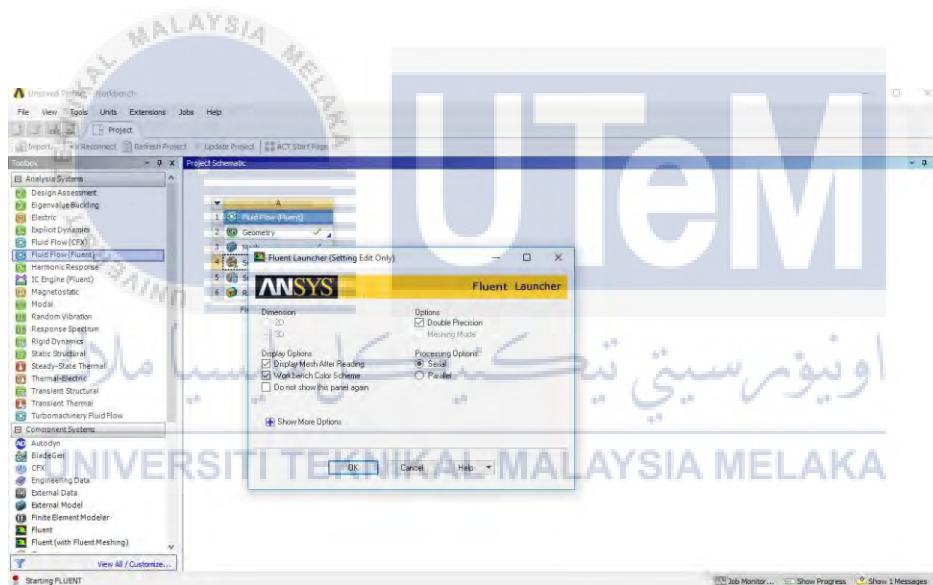
Figure 3.16: example of ANSYS fluent launcher
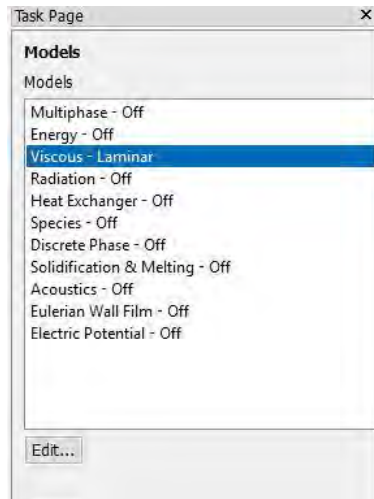
Figure 3.17: example of the model setup
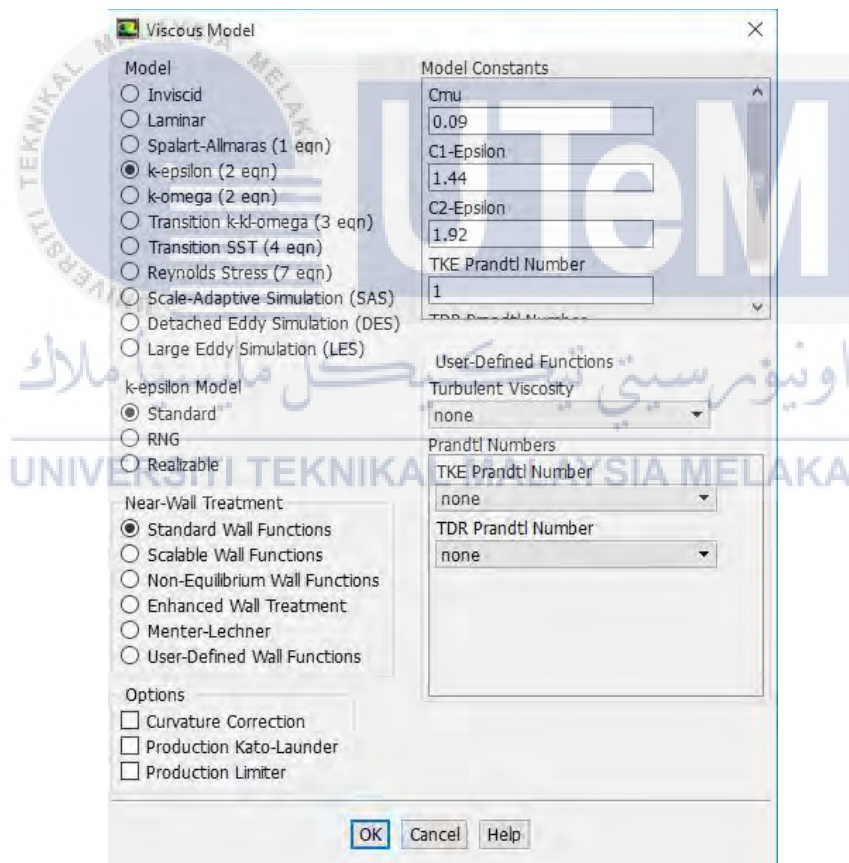
Figure 3.18: example of viscous model setup

In solution, the solution method need to be setup, the pressure for the solution had been set as standard pressure. For momentum, kinetic energy, and dissipation rate of the turbulent, the second order upwind option had been choosing for this project. On the monitor option, the
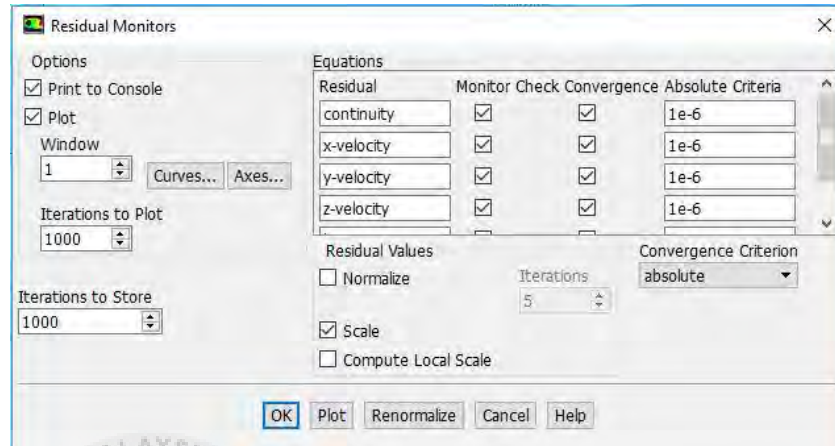
Figure 3.19: example of residual monitor

residual monitor need to be edit for iteration convergence purpose. All the residual value will be change into 1e-6, the figure below shows the example of the setting for the residual monitor. This project is focusing on the lift and drag for the air foil hence, the drag and lift monitor had been enable. On the drag and lift monitor, the plot, write and print check box need to be checked. After that, Hybrid initialization had been chosen in solution initialization and the initialize button need to be clicked. At the run calculation menu, the number iteration had been set into 10000 iterations and the calculation had been started. The residual graph had been shown at the console and the iteration had been stop once the graph had been convergence.

3.4   Result and Discussion

The result of the simulation can be generated after the calculation had been completed. From the result menu, the vector and streamline can be achieved by displaying those features. The analysis had been made based on the result that had been calculated by the software. If the

result is not reliable, the simulation had been run once again or the setup had been checked again if there any mistake that had been done during the setup for the simulation. The result and analysis had been further explained on chapter 4.

CHAPTER 4

RESULT AND DISCUSSION

4.1   Results

On this chapter, the discussion is focused on the result that had been obtained from the simulation. The simulation is involving the changes of angle of attack (AOA) by using the same type of blade profile (NACA 8415). The range of angle of attack (AOA) for this study are from -10º to +30º. The graph for lift and drag had been plotted to determine the point of stalling region. The simulation had been run in 2-dimensional geometry drawing. The inlet boundary condition for the blade are 680m/s at 500ºC (773K) and the fluid for this simulation is hot air. The inlet boundary condition parameter had been obtained from D. Villanueva and C. Maglasang (2015). The result and analysis are focusing on the stalling and the pattern of the flow around the blade profile.

4.1.1 Velocity and Pressure Contour

velocity   pressure

α = -10 deg

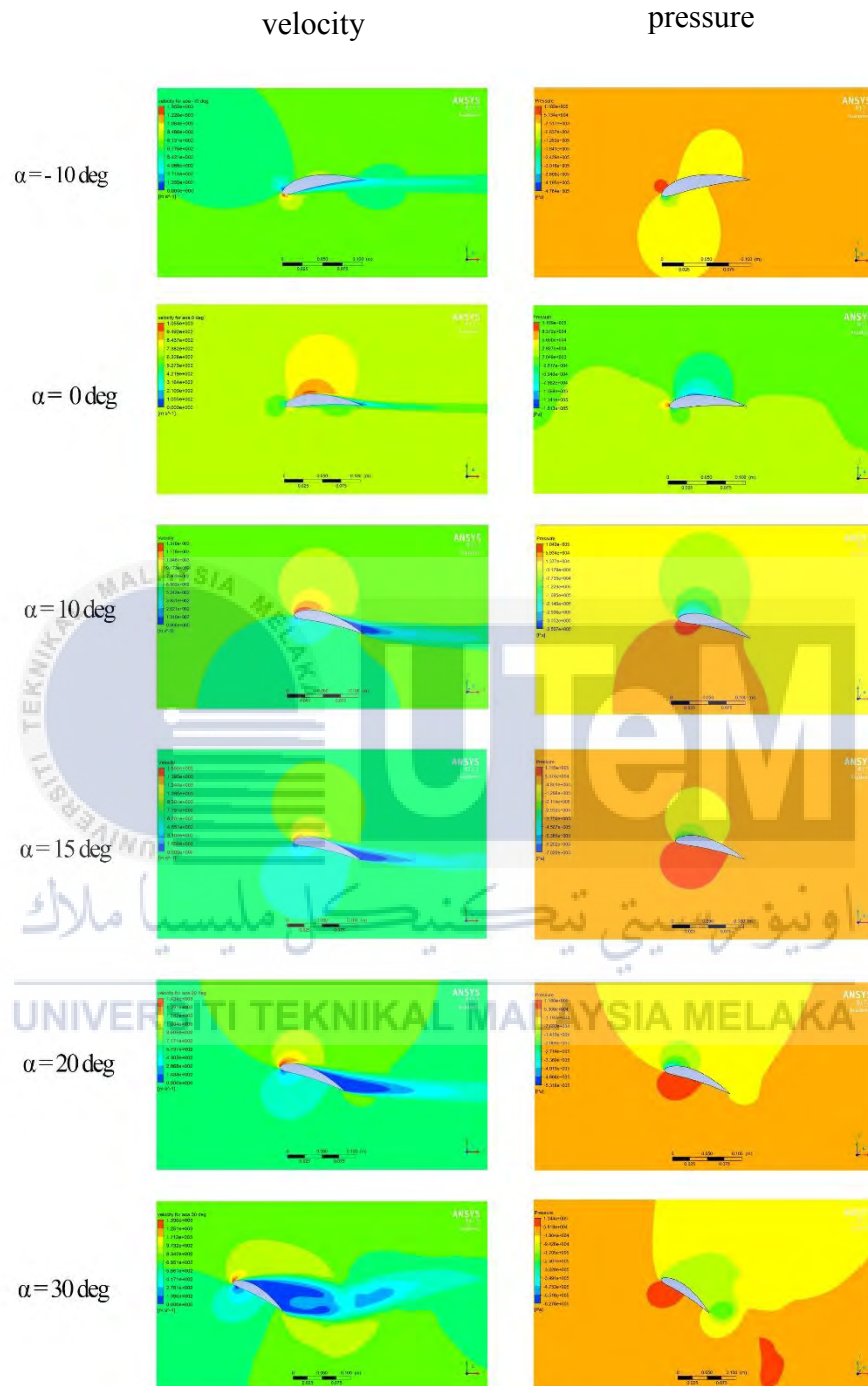α = 0 deg

α = 10 deg

α = 15 deg

α = 20 deg

α = 30 deg

Figure 4.1: velocity contour pattern at difference angle of attack (AOA)

Figure 4.1 show the contour pattern at a different angle of attack (AOA). At the angle of -10 degree, there is no separation occur. The higher velocity only can be found at the leading edge of the blade profile. After passing the leading edge, the flow is attached to the blade profile with a low velocity. From the pressure contour, it has been shown that the orange colour which indicates the pressure around the test section is higher and the pressure is decrease slightly when approaching the upper chamber and the lower chamber of the blade profile. At the leading edge of the profile, the contour has shown a red colour which indicates the higher pressure at the trailing edge. At the lower chamber leading edge, it can be see that the small region that have a lower pressure which is indicates as a green colour. According to this pressure contour it can be said that, the lift coefficient is still higher comparing to the drag coefficient.

When the angle of attack (AOA) increasing to 0 degree. The contour has shown the higher velocity at the upper chamber of the blade profile. The velocity decreasing when it is far from the blade profile. The pressure contour for this blade profile had shown a constant pressure at the entire of the test section. The higher pressure only can be found at the leading edge of the blade profile for all cases. This is due to the impact of the inlet velocity to the blade profile and it had been separated at the specific stagnation point. The lowest pressure region can be found only at middle of the upper chamber of the blade profile. From -10 degrees to the 0 degree angle of attack (AOA), the production of the laminar separation bubble or separation of the flow are not present at this angle.

At angle of 10 degree, the separation flow has started to appear. The velocity is higher at the leading edge of the blade profile and the low velocity at the trailing edge. The higher pressure had surround the lower chamber region of the blade profile at this stage, the lift coefficient of the blade profile is at the highest point compared to the other angle of attack

44

(AOA). The separation flow had been grown up when the angle of attack (AOA) is increasing to the 15 degrees. At the angle of attack of 15 degrees, the flow had been separated at the mid-chord of the blade profile. The turbulence region is bigger compared to separation flow at the previous angle. At the lower chamber region, the flow is attached at the trailing edge of the blade profile. At the upper chamber, the velocity is higher at the leading edge of the blade profile. The pressure contour had shown the higher pressure at the lower chamber of the blade profile. At this instance, the blade is at the maximum of the lift coefficient. The blade starts to lose the lift after the angle of attack of 15 degree. By referring figure 4.1 it can be see that the upper chamber of the blade profile had been surround by higher pressure contour. The higher pressure at the upper chamber of the blade profile had produced a down force to the blade, thus, it had cause the blade to lose the lift coefficient and increase the drag coefficient.

The production of the laminar separation bubble had been found at the angle of 30 degree. At this stage, the separation flow had cover all the upper chamber of the blade profile. The laminar separation bubble had been produce when the flow leaves the blade profile. The pressure contour show, the large yellow region at the upper chamber of the blade profile. The higher-pressure region at the lower chamber of the blade profile, had been decreases. The region of the higher pressure starts at the leading edge until the mid-chord of the blade profile and it lose the pressure through the trailing edge of the blade profile. At the upper chamber, the pressure contour had shown the vorticity that had been produced at the trailing edge, the indicator had shown the negative value of pressure this is means that, the flow is circulating at the trailing edges and produce a vorticity with a suction pressure.

45

4.1.2 Lift and Drag Coefficient
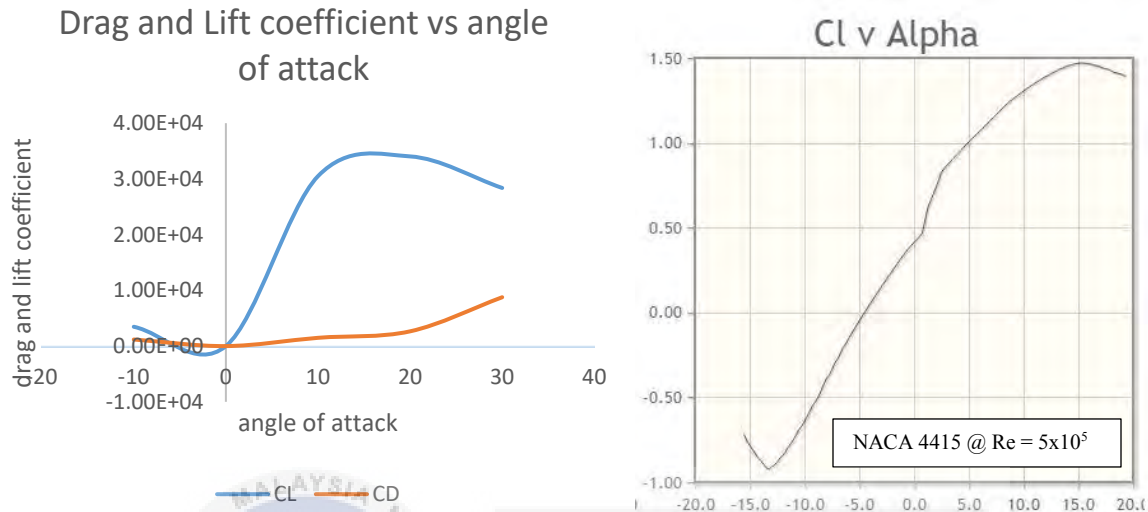
Figure 4.2: graph for coefficient lift and drag against angle of attack (AOA) for NACA 8415 and NACA 4415 (adapt from airfoiltools.com)

The graph shows the curve for the C_L and C_D graph against the angle of attack (AOA). At the -10 degrees, the lift coefficient is higher than the drag coefficient, as the angle of attack (AOA) increase towards the 0 degree, the lift coefficient starts to decrease to the negative value, this is because the flow is not steady during this angle. At the 0 degree, the coefficient of lift and drag value are zero which means the flow on the blade profile is steady and there is no pressure difference on the upper chamber and lower chamber of the blade profile. At this stage, the lift coefficient is equal to the drag coefficient. There is no separation flow occur at this angle, because of the flow is steady from the leading edge to the trailing edge.

The coefficient of lift starts to increase from 0 to 15 degrees and it lose the lift coefficient after the 15 degrees. At this stage, the flow separation started to present when the angle is increasing. The production of turbulence flow starts to produce at the trailing edge of the blade

46

profile. The drag coefficient increasing gradually with the increasing angle of attack (AOA). By referring to the theory for the stalling phenomena, the stalling is the reduction of the lift coefficient when the angle of attack (AOA) increase (crane and dale, 1997). Thus, the stalling point for this blade profile at angle of 15 degree. This is because, after angle of 15 degree the lift coefficient keeps decreasing until the angle of 30 degree. As we can see at the contour velocity (figure 4.1), at angle of 10 degree the attachment of separation flow is at the trailing edge had cover the quarter of the blade profile from the trailing edge and at the angle of 20 degree, the attachment of separation flow had completely covered the upper chamber of blade profile. The flow only steady at the trailing edge, once the flow is separated at the trailing edge stagnation point the flow start to produce unsteady turbulence flow.
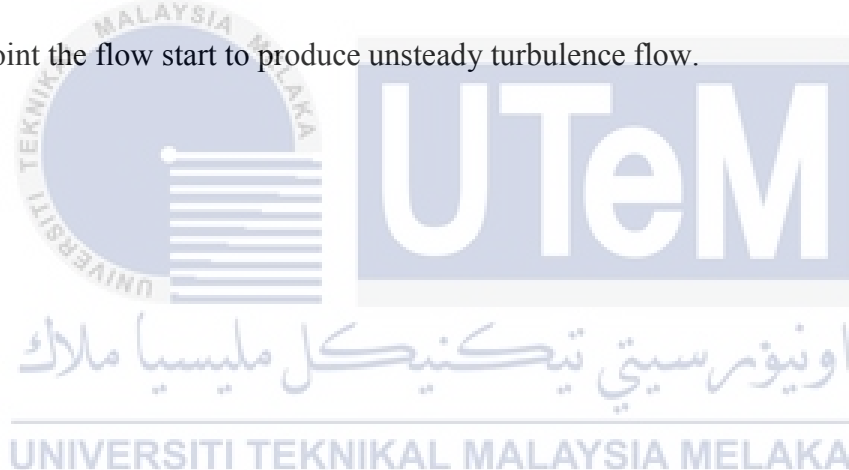
4.1.3 Velocity vector and Streamline
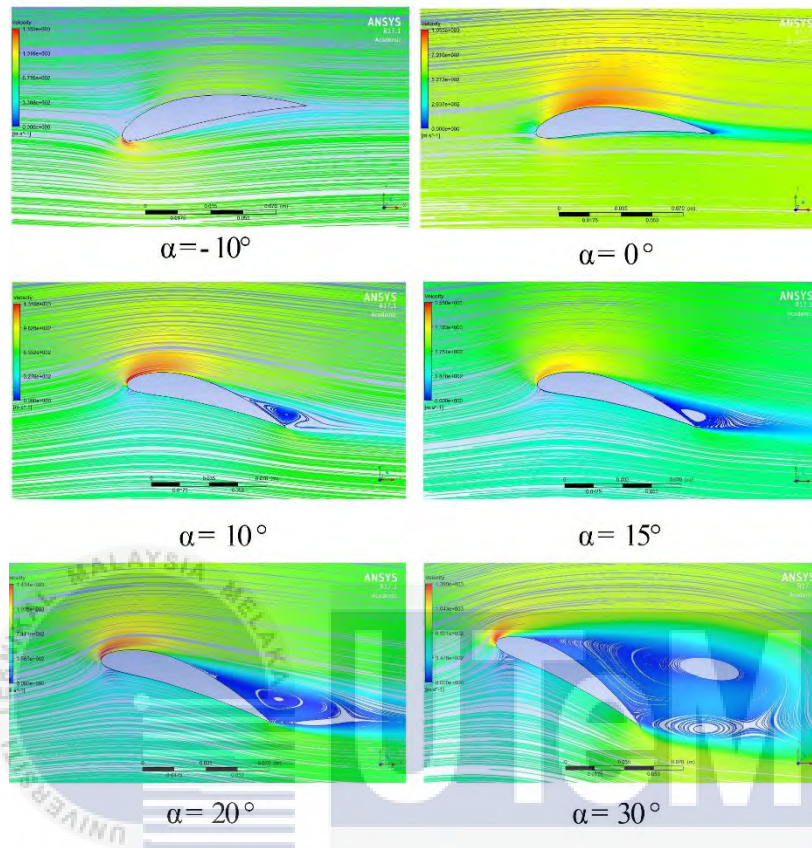
Figure 4.3: streamline velocity at various angle of attack (AOA)

The streamline velocity pattern is very important in computational fluid dynamics (CFD) to determine the flow pattern on the simulation. From the streamline velocity, the type of flow can be determined whether laminar, turbulent or transition flow. Figure 4.3, shows the streamline pattern for NACA 8415 blade profile. At angle -10 to 0 degree the pattern is almost the same, the separation point for each angle are different. For example, the separation point for angle -10 degree the separation at the upper chamber of the blade profile but when the angle is increased to 10 degrees, the separation point is located at the lower chamber of the blade profile. The flow pattern at this stage can be stated as transition because some of the angle had produce a small separation at the trailing edge of the blade profile.

The formation of laminar separation bubble is started to produce at the trailing edge angle of 10 degree. The laminar separation bubble keeps growing from 10 degrees to 30 degrees. Due to the growing of laminar separation bubble, the drag coefficient starts to increase and the lift coefficient start to decrease.

4.2 Discussion

The simulation had been done by using ANSYS fluent and some of the parameter had been setup as a constant variable for all cases. The manipulated variable for this simulation only the angle of attack (AOA) for the blade profile. The angle of attack (AOA) start from -10 degrees and had been increase +10 degrees for each simulation until it achieves +30 degrees. The pressure had been setup as a default pressure which is at 101kpa. The inlet velocity is 680 m/s (6500RPM) and the temperature is 500°C, this parameter had been extracted from study conduct by Villanueva & Maglasang, (2015).

From the result that had been obtained, the blade starts to stall at the angle of +15° (see fig 4.4). At this angle, the blade profile starts to lose the lift coefficient. The attachment of laminar separation bubble start to appear at the angle of +10° and the laminar separation bubble start to grow when the angle of attack (AOA) is increase. Until at the angle of +30° the laminar separation bubble start to produce more bubble at the trailing edge. The laminar separation bubble had been attached together because of the vorticity that had been produced by the new laminar separation bubble. Thus, the old laminar separation bubble had been attached together. At this stage, it can be concluded that the blade profile had been completely stalling.
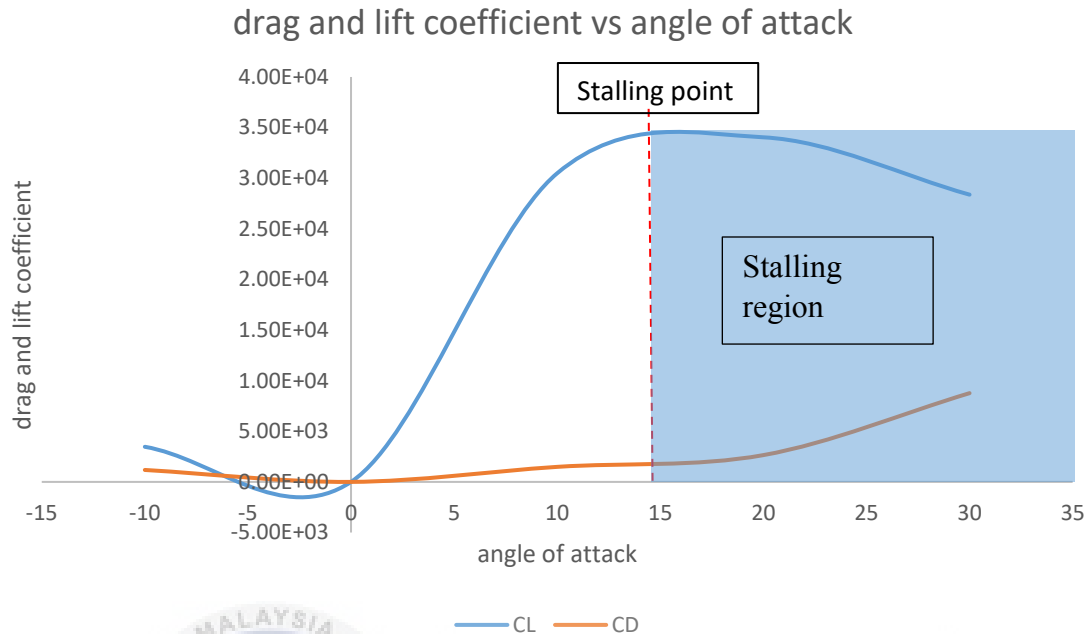
drag and lift coefficient vs angle of attack

Figure 4.4: determination of stalling point and stalling graph

By referring to the figure 4.5, starting from the angle of attack of +10° the flow start producing the backflow at the trailing edge of the blade profile but at the α = +10° and α = +20° the formation of the backflow only can be seen at the tip of the trailing edge. This is due to the some of the flow had been attached to the laminar separation bubble. At the angle of α = +30°, the backflow position had climbing up from the tip of the trailing edge this is because, the old laminar separation bubble had been attached together with the new laminar separation bubble. The separation had been attached together after it passed the vorticity. At the velocity for the vorticity increases when the flow is nearer to the blade profile and escaped from the laminar separation bubble. The slower velocity at the midpoint of vorticity will produce a high suction pressure at the midpoint. Figure 4.6 had shown the pressure at the trailing edge for α = 10°,20° and 30°. From the figure, it can be see that the pressure region at the trailing edge are getting bigger when the angle of attack had been increased. For α = 30°, it had been seen that, there is

50

a small green pressure region leaving the trailing edge. This region is called the suction region where the flow had been moves in circular direction after leaving the trailing edge of the blade profile. It can also be seen, the small orange region at the bottom of the pressure contour region. This region is the attachment region for the laminar separation bubble. The separation had been attached back together after the flow leaving the circulation flow. The pressure become higher at that particular region because of the two-attachment laminar separation bubble flow had leave the circular flow at the same direction. This is due to the flow circulation for both laminar separation bubble is counter to each other.
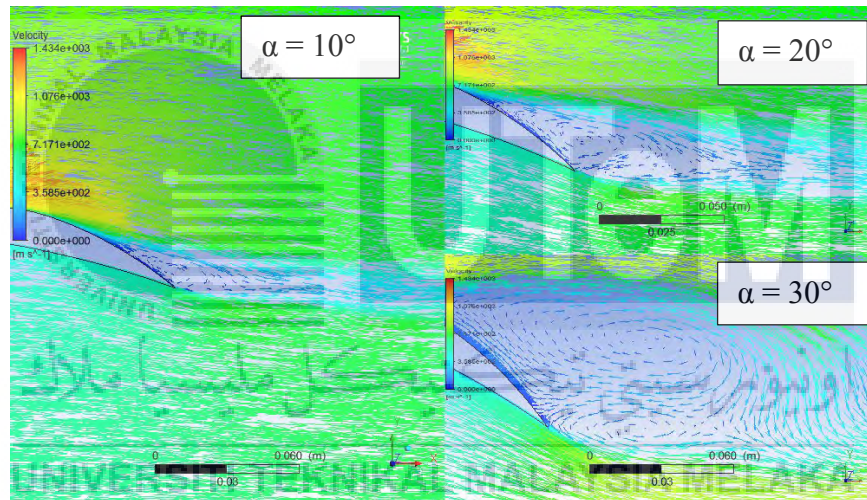

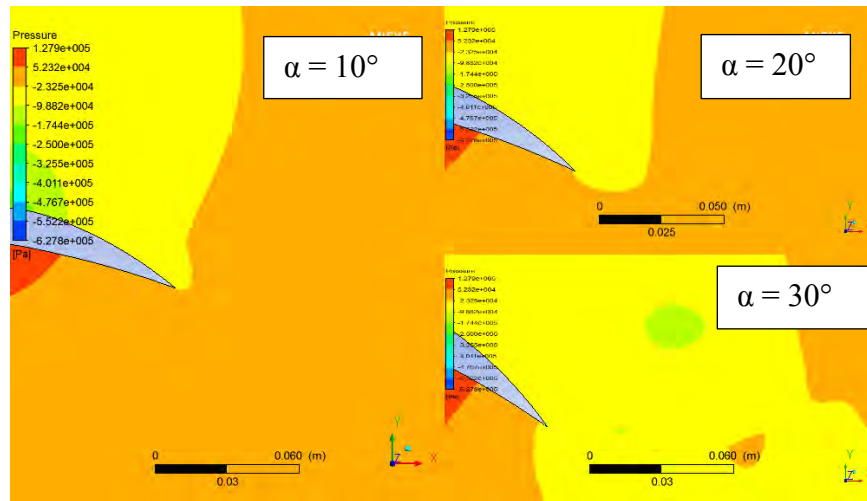Figure 4.5: vector velocity at trailing edge α = 10°, 20°, 30°

Figure 4.6: pressure contour at the trailing edge α = 10°,20°,30°

CHAPTER 5

CONCLUSION

5.1 Conclusion and Recommendation

From the analysis, it can be concluded that the higher angle of attack (AOA) had cause the stalling phenomena to happen at the blade profile. This phenomenon had reduced the lift coefficient for the blade profile and increase the drag coefficient for the blade profile thus, it had cause the efficiency and performance for the steam turbine had be reduced. The stalling angle can be increases by reduce the inlet velocity, if the flow is keep attaching to the blade profile, the blade had not face the stalling phenomena because the flow had not separated. This study had been carried out to determine the stalling point for NACA 8415 profile. The study had been conduct by using CFD simulations at six different angle of attack (AOA) with the constant pressure and inlet velocity. The analysis had been run in 2-dimensional analysis with the meshing that had been set as finest as it can to ensure the accuracy in data. The validation for the data that had been obtained had been compared to the NACA 4415 blade profile to determine whether the result is significant or not.

The drag and lift coefficient can be obtained from the ANSYS fluent software. The value of drag and lift coefficient from the simulation had been taken and the drag and lift coefficient vs angle of attack (AOA) graph had been plotted to determine the stalling point. From the result that had been obtained, the blade starts to stall at the angle of 15°. When the stalling point had been determined, the angle of attack (AOA) after the 15° had been considered as a stalling region

for NACA 8415 blade profile. The NACA 8415 plot had been compared to the NACA 4415 plot to see the difference of the results. The different between both profile are only at the percentage of maximum chamber. The graph on figure 4.2 had shown the comparison for both blade profile.

This study can be continued to make an improvement on the result for the stalling region. On this study, the angle had been increase +5° for each simulation and the inlet velocity is at 680m/s. Some of recommendation can be recommend for those who want to further this study. One of the parameter that can be improved from this study is reduced the increment angle for each simulation less than +5°, by doing this, all separation flow can be see clearly and the exact stalling point can be determined. Second, decrease the value for the inlet velocity to see whether the angle for stalling region can be decrease or not. This is because when the inlet velocity is slower the flow will keep attached at the blade profile form the leading to the trailing edge thus, it will produce the turbulence flow after it leave the trailing edge. Last but not least, this analysis is on 2-Dimensional analysis, for further this study, the actual 3-Dimensional analysis with the twisted angle for the blade profile can be recommended as the type of the analysis for this study.

REFERENCES

Ac kel, H. H., & Genc, M. S. (2016). Flow control with perpendicular acoustic forcing on NACA 2415 aerofoil at low Reynolds numbers. Proceedings of the Institution of Mechanical Engineers, Part G: Journal of Aerospace Engineering, 230(13), 2447–2462. doi:10.1177/0954410015625672.

Airfoiltools – NACA 4415 CL vs AOA. retrieved April 1,2017 from http://airfoiltools.com/airfoil/details?airfoil=naca4415-il.

Airfoiltools-coordinate generator for NACA 8415.retrieved February 22,2017 from http://airfoiltools.com/airfoil/details?airfoil=m27-il.

Akbari, M. H., & Price, S. J. (2003). Simulation of dynamic stall for a NACA 0012 airfoil using a vortex method. Journal of Fluids and Structures, 17(6), 855–874. doi:10.1016/s0889-9746(03)00018-5.

Almohammadi, K. M., Ingham, D. B., Ma, L., & Pourkashanian, M. (2015). Modeling dynamic stall of a straight blade vertical axis wind turbine. Journal of Fluids and Structures, 57, 144–158. doi:10.1016/j.jfluidstructs.2015.06.00.

Anand, K., & Sarkar, S. (2016). Features of a Laminar separated boundary layer near the leading-edge of a model Airfoil for different angles of attack: An experimental study. Journal of Fluids Engineering, 139(2), 021201. doi:10.1115/1.4034606.

ANSYS. (2016). ANSYS fluent: CFD simulation. Retrieved December 16, 2016, from http://WWW.Fluent.com.

Chaluvadi, V. S. P., Kalfas, A. I., Hodson, H. P., Ohyama, H., & Watanabe, E. (2003). Blade row interaction in a high-pressure steam turbine. Journal of Turbomachinery, 125(1), 14. doi:10.1115/1.1518504.

Choudhry, A., Arjomandi, M., & Kelso, R. (2015). Methods to control dynamic stall for wind turbine applications. Renewable Energy, 86, 26–37. doi:10.1016/j.renene.2015.07.097.

Costes, M., Richez, F., Le Pape, A., & Gavériaux, R. (2015). Numerical investigation of three-dimensional effects during dynamic stall. Aerospace Science and Technology, 47, 216–237. doi:10.1016/j.ast.2015.09.025.

Crane, Dale: Dictionary of Aeronautical Terms, third edition, page 486. Aviation Supplies & Academics, 1997. ISBN 1-56027-287-2.

Danish wind (2000, august 6). Aerodynamics of Wind Turbines: Stall and Drag [web log post]. Retrieved October, 20, 2016, http://ele.aut.ac.ir/~wind/en/tour/wtrb/stall.htm.

Geissler, W., & Haselmeyer, H. (2006). Investigation of dynamic stall onset. Aerospace Science and Technology, 10(7), 590–600. doi:10.1016/j.ast.2006.05.001.

Gharali, K., & Johnson, D. A. (2012). Numerical modeling of an S809 airfoil under dynamic stall, erosion and high reduced frequencies. Applied Energy, 93, 45–52. doi: 10.1016/j.apenergy.2011.04.037.

Hoo, E., Do, K. D., & Pan, J. (2005). An investigation on the lift force of a wing pitching in dynamic stall for a comfort control vessel. *Journal of Fluids and Structures*, *21*(8), 707–730. doi:10.1016/j.jfluidstructs.2005.08.009.

Huang, D., Li, J., & Liu, Y. (2015). Airfoil dynamic stall and Aeroelastic analysis based on multi-frequency Excitation using CFD method. Procedia Engineering, 99, 686–695. doi:10.1016/j.proeng.2014.12.590.

56

Liu, P., Yu, G., Zhu, X., & Du, Z. (2014). Unsteady aerodynamic prediction for dynamic stall of wind turbine airfoils with the reduced order modeling. Renewable Energy, 69, 402–409. doi:10.1016/j.renene.2014.03.066.

Lucius, A., & Brenner, G. (2010). Unsteady CFD simulations of a pump in part load conditions using scale-adaptive simulation. International Journal of Heat and Fluid Flow, 31(6), 1113–1118. doi:10.1016/j.ijheatfluidflow.2010.06.005.

Menter, F. R. (1994). Two-equation eddy-viscosity turbulence models for engineering applications. AIAA Journal, 32(8), 1598–1605. doi:10.2514/3.12149.

Morgado, J., Vizinho, R., Silvestre, M. A. R., & Páscoa, J. C. (2016). XFOIL vs CFD performance predictions for high lift low Reynolds number airfoils. *Aerospace Science and Technology*, *52*, 207–214. doi:10.1016/j.ast.2016.02.031.

Numerical simulation of the 3D viscous flow in the exhaust casing of a low -pressure steam turbine by x.xu, s.kang and CH.hirsch (2001).

Pellegrino, A., & Meskell, C. (2013). Vortex shedding from a wind turbine blade section at high angles of attack. Journal of Wind Engineering and Industrial Aerodynamics, 121, 131–137. doi:10.1016/j.jweia.2013.08.002.

Rama S. R. Gorla, Aijaz A. Khan (2003). Turbomachinery design and theory. Marcel Dekker, Inc.

Sauret, E., & Gu, Y. (2014). Three-dimensional off-design numerical analysis of an organic Rankine cycle radial-inflow turbine. Applied Energy, 135, 202–211. doi: 10.1016/j.apenergy.2014.08.076.

Tutorvista.com-The Reynold number formula. retrieved May 15,2017 from http://formulas.tutorvista.com/physics/reynolds-number-formula.html?view=sample.

Villanueva, M. D., & Maglasang, J. C. (2015). Computational and Experimental Study of a Gas/Steam Turbine — Derivative Axial Flow Impulse-Type Hydraulic Turbine. International Journal of Materials, Mechanics and Manufacturing, 3(2), 86-91. doi:10.7763/ijmmm.2015.v3.172.

Wang, Q., Zhao, Q., & Wu, Q. (2015). Aerodynamic shape optimization for alleviating dynamic stall characteristics of helicopter rotor airfoil. Chinese Journal of Aeronautics, 28(2), 346–356. doi:10.1016/j.cja.2014.12.033.

Wang, S., Ingham, D. B., Ma, L., Pourkashanian, M., & Tao, Z. (2012). Turbulence modeling of deep dynamic stall at relatively low Reynolds number. Journal of Fluids and Structures, 33, 191–209. doi:10.1016/j.jfluidstructs.2012.04.011.

Yunus A. Cengel, John M. Cimbala (3rd Ed.) (2014). *Fluid Mechanics.* Mc Graw Hill education.